Climate
of the Past

Biotic response of plankton communities to Middle to Late Miocene monsoon wind and nutrient flux changes in the Oman margin upwelling zone

Gerald Auer[1]**, Or M. Bialik**[2,3]**, Mary-Elizabeth Antoulas**[1]**, Noam Vogt-Vincent**[4]**, and Werner E. Piller**[1]

[1]Department of Earth Sciences, University of Graz, NAWI Graz Geocenter, Heinrichstrasse 26, 8010 Graz, Austria
[2]Institute of Geology and Palaeontology, University of Muenster, Corrensstr. 24, 48149 Münster, Germany
[3]Dr. Moses Strauss Department of Marine Geosciences, The Leon H. Charney School of Marine Sciences,
University of Haifa, Carmel 31905, Israel
[4]Department of Earth Sciences, University of Oxford, Oxford, UK

Correspondence: Gerald Auer (gerald.auer@uni-graz.at) and Or M. Bialik (obialik@uni-muenster.de)

Abstract. Understanding past dynamics of upwelling cells is an important aspect of assessing potential upwelling changes in future climate change scenarios. Our present understanding of nutrient fluxes throughout the world's oceans emphasizes the importance of intermediate waters transporting nutrients from the Antarctic divergence into the middle and lower latitudes. These nutrient-rich waters fuel productivity within wind-driven upwelling cells in all major oceans. One such upwelling system is located along the Oman margin in the western Arabian Sea (WAS). Driven by cross-hemispheric winds, the WAS upwelling zone's intense productivity led to the formation of one of the most extensive oxygen minimum zones known today.

In this study covering the Middle to Late Miocene at Ocean Drilling Program (ODP) Site 722, we investigate the inception of upwelling-derived primary productivity. This study presents new plankton assemblage data in the context of existing model- and data-based evidence constraining the tectonic and atmospheric boundary conditions for upwelling in the WAS. With this research, we build upon the original planktonic foraminifer-based research by Dick Kroon in 1991 as part of his research based on the ODP LEG 117.

We show that monsoonal winds likely sustained upwelling since the emergence of the Arabian Peninsula after the Miocene Climatic Optimum (MCO) ∼ 14.7 Ma, with fully monsoonal conditions occurring since the end of the Middle Miocene Climatic Transition (MMCT) at ∼ 13 Ma. How-ever, changing nutrient fluxes through Antarctic Intermediate and sub-Antarctic Mode Waters (AAIW/SAMW) were only established after ∼ 12 Ma. Rare occurrences of diatom frustules correspond to the maximum abundances of *Reticulofenestra haqii* and *Reticulofenestra antarctica*, indicating higher upwelling-derived nutrient levels. By 11 Ma, diatom abundance increases significantly, leading to alternating diatom blooms and high-nutrient-adapted nannoplankton taxa. These changes in primary producers are also well reflected in geochemical proxies with increasing $\delta^{15}N_{org.}$ values ($> 6\,‰$) and high organic carbon accumulation. These proxies provide further independent evidence for high productivity and the onset of denitrification simultaneously.

Our multi-proxy-based evaluation of Site 722 primary producers provides evidence for a stepwise evolution of Middle to Late Miocene productivity in the western Arabian Sea for the first time. The absence of a clear correlation with existing deep marine climate records suggests that both local wind patterns and intermediate water nutrient changes likely modulated productivity in the western Arabian Sea during the Middle to Late Miocene. Finally, we show that using a multi-proxy record provides novel insights into how plankton responded to changing nutrient conditions through time in a monsoon-wind-driven upwelling zone.

1 Introduction

Within coastal upwelling zones, wind-driven Ekman transport brings nutrient-rich deep water into the photic zone (Woodward et al., 1999). This process supports enhanced primary productivity in the surface ocean. This increased productivity supports a large biomass across the entire food chain, reaching far afield from the core of the upwelling zone. In addition, the high productivity in upwelling zones produces a significant amount of marine snow (both organic and inorganic), which sinks through the water column. As the organic particulates fall, they become partially remineralized, consuming oxygen and forming an oxygen-depleted zone. However, the flux of organic matter is so large that a significant volume of organic matter reaches and accumulates on the seafloor (e.g. Suess, 1980; Rixen et al., 2019a, b).

Upwelling zones affect the marine carbon cycle by sequestering carbon and exchanging carbon between the ocean and the atmosphere via the dissolved inorganic carbon system and pCO$_2$ changes (Rixen et al., 2006; Krapivin and Varotsos, 2016; Wang et al., 2015). Increased photosynthesis-driven primary productivity during upwelling produces high organic carbon export from the photic zone into the deep sea through the organic carbon pump (Volk and Hoffert, 1985; Ridgwell and Zeebe, 2005). Primary producers account for most of the biomass in upwelling zones, with phytoplankton accounting for $> 80\%$ of the particulate organic carbon (Head et al., 1996). Calcification by these primary producers and heterotrophic organisms feeding on them is a further important contributor to the inorganic carbon cycle of the oceans (Falkowski, 1997; Raven and Falkowski, 1999; Ridgwell and Zeebe, 2005; Millero, 2007). However, the productivity of coastal upwelling zones highly depends on atmospheric conditions as they are primarily wind driven. Consequently, wind-driven upwelling further constitutes a direct intersection between the oceans and the atmosphere. Hence, changes in average wind speeds are directly responsible for the intensity and size of upwelling zones (Dugdale, 1972; Shimmield, 1992; Tudhope et al., 1996; Balun et al., 2010). Therefore, these atmospheric processes may also influence the community structure of primary producers and consumers within the area affected by upwelling.

Today, the western Arabian Sea (WAS) upwelling is one of the most productive marine regions (Lee et al., 1998; Honjo et al., 1999; Munz et al., 2017; Rixen et al., 2019b). Its high productivity and organic matter flux fuels the Arabian Sea oxygen minimum zone (OMZ), which extends southwards from the Oman margin between 200 and 1000 m water depth, reaching as far south as 10° N (Morrison et al., 1998; McCreary et al., 2013), making it one of the largest oxygen-deficient zones in the modern ocean.

Primary productivity in the WAS is furthermore driven by seasonal winds flowing northward along the eastern coast of Africa (Currie et al., 1973; Rixen et al., 2019a) as an extension of the Somali and Findlater jets (Sarr et al., 2022; Find-

later, 1969). Upwelling in the WAS is thus directly forced by the cross-hemispheric circulation system of the Indian Summer Monsoon (Findlater, 1969; Woodward et al., 1999; Basavani, 2013; Sarr et al., 2022). The prevailing southwesterly winds in the region during the summer months result in the displacement of large water masses (Tudhope et al., 1996; Schott and McCreary, 2001; Schott et al., 2009; Lahiri and Vissa, 2022), resulting in pronounced, intense upwelling peaks during the summer monsoon season (Lee et al., 1998; Honjo et al., 1999; Rixen et al., 2019b). During the Northern Hemisphere winter, the prevailing wind direction in the Arabian Sea reverses as a weaker and dryer winter monsoon becomes established (Gadgil, 2018). The northeasterly winter monsoon winds result in an additional, albeit less pronounced, productivity spike in the region (Madhupratap et al., 1996; Munz et al., 2015, 2017; Rixen et al., 2019b). Between these two regimes – the inter-monsoon season – weak and variable winds dominate, permitting the establishment of well-stratified regions in the WAS that exhibit oligotrophic surface water conditions. The shift between the different conditions generates a complex pattern of abundance shifts between nutrient-adapted and primarily mesotrophic but potentially even oligotrophic phytoplankton communities. This dynamic impact of changes in wind regimes and upwelling intensity on plankton communities in the WAS is well established for the modern period (Schiebel et al., 2004).

In the Arabian Sea, significant variability in productivity has been identified over Pleistocene glacial–interglacials. For example, higher productivity in the Late Pleistocene is associated with interglacial periods (Schubert et al., 1998; Pourmand et al., 2007; Avinash et al., 2015; Naik et al., 2017). Conversely, these climatically driven changes in primary productivity affect the volume of the oxygen minimum zone (OMZ) and the intensity of denitrification in the region (Gaye et al., 2018). An OMZ is the result of the complete consumption of dissolved oxygen in the water column due to the microbial degradation of sinking organic matter. Hence, OMZ strength is generally related to the strength of primary productivity and thus organic matter flux within the overlying upwelling cell (Dickens and Owen, 1994; McCreary et al., 2013; Stramma et al., 2008)

Based on current records, the earliest activity within the upwelling zone may have occurred earlier in the Burdigalian (Bialik et al., 2020b). However, it was not until connectivity to the proto-Mediterranean was terminated and the Arabian Peninsula began to emerge that the regional geographic configuration allowed the establishment of a strong upwelling cell driven by the Findlater Jet (Rögl, 1999; Reuter et al., 2013; Harzhauser et al., 2007; Bialik et al., 2019; Sarr et al., 2022). After the Miocene Climatic Optimum (MCO) ~ 14 Ma (Flower and Kennett, 1994; Frigola et al., 2018; Sosdian and Lear, 2020), global cooling resumed, and a stable, upwelling zone and a sustained OMZ resembling present-day conditions were reported to have established in

the WAS (Kroon et al., 1991; Zhuang et al., 2017; Bialik et al., 2020a).

Modelling studies suggest that the inception of upwelling and the WAS was closely linked to the tectonic evolution of the Arabian Peninsula, which resulted in water displacement by the Findlater Jet along a newly emergent coastline of Oman (Zhang et al., 2014; Sarr et al., 2022). Therefore, the uplift of the Arabian Peninsula is now seen as the dominant controlling factor for the inception of monsoonal upwelling in the WAS, which is now also viewed as largely separate from prevailing monsoonal rainfall patterns (Sarr et al., 2022). After the tectonic configuration of the Arabian Peninsula was in place, the cross-hemispheric wind patterns of the South Asian Monsoon were subsequently able to drive upwelling in the WAS in a near-modern configuration since the Middle Miocene Climatic Transition (MMCT) (Bialik et al., 2020a; Betzler et al., 2016; Gupta et al., 2015).

Evidence suggests that strong upwelling in the Arabian Sea first occurred between the Middle and Late Miocene (Kroon et al., 1991; Huang et al., 2007a; Tripathi et al., 2017; Zhuang et al., 2017; Bialik et al., 2020a; Alam et al., 2022). To date, manganese redirection – i.e. the depletion of Mn in the sedimentary record due to Mn reduction in the water column and subsequent advective transport to the edges of the OMZ – is one of the most used proxies to define OMZs and their past extent within the ocean (Dickens and Owen, 1994). Together with sedimentological facies and micropaleontological studies (Dickens and Owen, 1999; Gupta et al., 2004) these methods have been used effectively to track the size of the OMZ throughout the Indian Ocean and by proxy also the intensity of upwelling-derived primary productivity. $\delta^{15}N$ values $> 6\text{\textperthousand}$ are seen as possible indicators for significant water column denitrification within the OMZ based on the approach of Tripathi et al. (2017). Bialik et al. (2020a) applied this approach to a Middle to Late Miocene interval at Site 722, showing that upwelling in the WAS may have sustained an OMZ strong enough for denitrification to occur as early as 11 Ma ago. However, these methods do not provide direct evidence how changing wind and nutrient levels have interacted to result in the observed OMZ pattern.

Following these lines of evidence, it can be summarized that WAS upwelling initiated during the Middle to Late Miocene during the MMCT, marked by cooling sea surface temperatures (SSTs) since $\sim 14.7\,\text{Ma}$ (Zhuang et al., 2017; Holbourn et al., 2014, 2015). Monsoonal winds subsequently intensified only after the MMCT at $\sim 13\,\text{Ma}$, in conjunction with OMZ expansion to the Maldives (Betzler et al., 2016) before reaching maximum intensity at $\sim 11\,\text{Ma}$ and potentially declining at $\sim 9\,\text{Ma}$ (Bialik et al., 2020a). Upwelling re-intensified later in the Miocene and oscillated into the Plio-Pleistocene (Kroon et al., 1991; Huang et al., 2007b; Gupta et al., 2015; Tripathi et al., 2017; Alam et al., 2022). The Serravallian upwelling intensification is accompanied by significantly increased biogenic silica accumulation across the northern Indian Ocean (Keller and Barron, 1983; Bal-

dauf et al., 1992). This biogenic silica bloom is dominated by siliceous plankton such as diatoms and radiolaria (Nigrini, 1991), indicating a sustained regime of high nutrient levels, which was able to support these primary producers (Blain et al., 1997; Schiebel et al., 2004; Mikaelyan et al., 2015).

The present study aims to better constrain the relationships and interactions between different plankton groups in the WAS within the context of the dynamic changes occurring in the Oman margin upwelling cell throughout the Middle to Late Miocene.

2 ODP Site 722 – site location, age model, and oceanographic setting

Ocean Drilling Project (ODP) Site 722 ($16°37'18.7''\,\text{N}$, $59°47'45.33''\,\text{E}$) lies offshore Oman on the Owen Ridge, a 300 km long and 50 km wide feature in the WAS (Fig. 1a). Site 722 is located at a water depth of 2027.8 m (Shipboard Scientific Party, 1989) at the edge of the present-day Oman upwelling zone (Fig. 1a) and lies below the core of the Indian Ocean Oxygen Minimum Zone (OMZ), with oxygen concentrations of $< 2\,\mu\text{mol}\,\text{kg}^{-1}$ persisting at between ca. 200–1000 m water depth (McCreary et al., 2013; Garcia et al., 2019).

The sedimentary cover at the site location comprises nannofossil, foraminifer, and diatom-rich pelagic oozes with silty clay (Shipboard Scientific Party, 1989; Rodriguez et al., 2014; Bialik et al., 2020a). Bialik et al. (2020a) recently published a revised age model for Site 722, which we will utilize throughout this study. The age–depth correlation relies on biostratigraphic information from the nannofossil assemblage data used in this study combined with existing shipboard data (Shipboard Scientific Party, 1989). The age model covers the study interval over the Middle Miocene to the Late Miocene (ca. 15.0–8.5 Ma, corresponding to a core depth of 276.62 to 404.94 m b.s.f.). Bialik et al. (2020a) published benchtop X-ray fluorescence (XRF)-based elemental data, total organic carbon content (TOC), and the calcite equivalent carbonate content in the analysed samples. These geochemical proxy data were subsequently used in conjunction with the nannofossil assemblage data to fully constrain the response of the assemblage to changing environmental conditions in the WAS upwelling zone.

The modern-day water mass configuration of the WAS (Fig. 1b) indicates that Indian Central Water (ICW) upwells in the upwelling region offshore Oman. The ICW result from a mixture of warm, highly saline Red Sea and Persian Gulf Waters (RSPGW), and sub-Antarctic Mode and Intermediate Waters (SAWM and AAIW, respectively). Modern oceanographic research suggests that SAMW/AAIW, which contributes to the ICW is the dominant source of nutrients in the Arabian Sea upwelling region today (Böning and Bard, 2009; Toggweiler et al., 2019; You and Tomczak, 1993; You, 1997, 1998). In addition, at present there also exists some contribu-
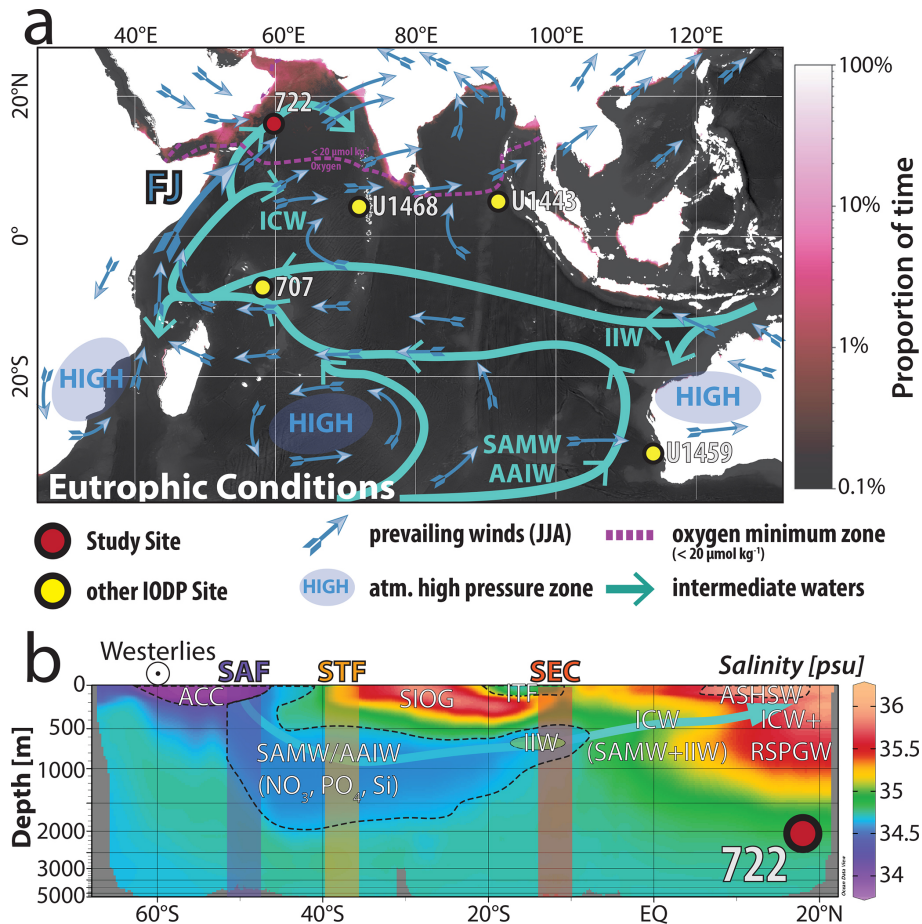
Figure 1. (a) Location map showing the study site ODP Site 722 and IODP Site U1468 and the prevalent summertime wind patterns following Bialik et al. (2020a). Generalized flow paths of dominant intermediate waters of the Indian Ocean follow You (1998) and Böning (2009). The present-day extent of the oxygen minimum zone is shown as a dashed pink line denoting oxygen concentrations $< 20\,\mu mol\,kg^{-1}$ at a water depth of 200 m (McCreary et al., 2013; Garcia et al., 2019). Eutrophication (magenta shading) data were provided by the EU Copernicus Marine Service Information using the Global Ocean Colour (Copernicus-GlobColour), Bio-Geo-Chemical, L4 (monthly and interpolated) from Satellite Observations (1997–ongoing); https://doi.org/10.48670/moi-00281. Shading represents gap-filled daily chlorophyll *a* product of Copernicus-GlobColour L4 (Gohin, 2011; Hu et al., 2012; Garnesson et al., 2019) and indicates the proportion of time spent in eutrophic conditions in the region based on the proportion of days (1998–2022) where chlorophyll *a* concentration exceeded a threshold of $7.3\,mg\,m^{-3}$ (derived from Carlson, 1977). The Python code used to generate the base map is available in the Supplement S1. **(b)** Salinity profile generated based on the World Ocean Atlas 2018 salinity data (Zweng et al., 2019) through the Indian Ocean from 65° S to 20° N. The plot was generated using Ocean Data View (Schlitzer, 2021). Water masses are differentiated based on their salinity signature outlined with dashed lines and labelled accordingly. Furthermore, major frontal systems and currents are also indicated. Abbreviations are as follows: Antarctic Intermediate Water (AAIW), Antarctic Circumpolar Current (ACC), Arabian Sea High-Salinity Water (ASHSW), Indian Central Water (ICW), Indonesian Intermediate Water (IIW), Red Sea/Persian Gulf Water (RSPGW), sub-Antarctic Mode Water (SAMW), southern Indian Ocean Gyre (SIOG).

tion of the Indonesian Intermediate Waters (IIW), the ICW in the WAS (Fig. 1a and b). Therefore, changes in the supply of these water masses are a critical aspect of understanding the region's past and likely future upwelling dynamics (Böning and Bard, 2009; Laufkötter and Gruber, 2018; Toggweiler et al., 2019). The Middle to Late Miocene was similar to the modern period (Bialik et al., 2019; Hall, 2012). However, the Indonesian Throughflow region's configuration remains largely enigmatic, with potentially large emergent island chains and extensive coral reefs between Aus-

tralia and South-East Asia (Hall, 2012). Deep and intermediate water exchange and thus IIW formation may thus have been restricted in the Miocene. If present, IIW likely would supply additional nutrients, including a significant amount of bioavailable silica, to the upwelling zone in the WAS (You and Tomczak, 1993; You, 1997). Waters in the WAS therefore represent a mixture of SAMW/AAIW and IIW with ICW, which later intermix with the regionally formed RSPGW (Böning and Bard, 2009; Toggweiler et al., 2019).

3 Methods

3.1 Nannofossil and siliceous fragment quantification

We produced smear slides from 71 freeze-dried samples taken from Hole 722B (Supplement S2) following the quantitative drop technique of Bordiga et al. (2015). On each slide, at least 47 field views were counted until at least 300 specimens were recorded or until over 190 field views were reached for samples containing very low abundances. During counting, nannofossils were identified to the species level whenever possible. The occurrence of diatom frustules (including pennate and centric forms), as well as other biogenic silica fragments (including silicoflagellates and radiolarian fragments), were quantitatively recorded without further taxonomic identification (Supplement S2). All recorded nannofossil taxa, as well as the siliceous skeletal fragments (including diatoms, silicoflagellates and radiolarian fragments), were then converted into absolute abundances per gram of sediment, according to Bordiga et al. (2015), with portions of the dataset already published (Bialik et al., 2020a). In addition to the above-described quantification, the high amount of biogenic silica recorded in some sections often dilutes absolute nannofossil abundances. We calculated nannofossil and diatom fluxes to alleviate the potential dilution of nannofossil abundance due to high biogenic silica fluxes for the studied interval (see Sect. 3.5).

3.1.1 Taxonomic remarks

We relied on the Nannotax3 website (Nannotax 3, 2023) for detailed taxonomic reference and identification. In addition, taxonomic identification followed the concepts outlined in Perch-Nielsen (1985) and Young (1998), the Handbook of Calcareous Nannoplankton 1–5 (Aubry, 1984, 1988, 1989, 1990, 1999), and the compilation on the taxonomy of the order Discoasterales by Aubry (2021).

For subsequent ecological interpretations, we combined the identified *Reticulofenestra* morphotypes into three size bins of small ($< 3\,\mu m$), medium (3–$5\,\mu m$), and large ($> 5\,\mu m$). There is some debate regarding the taxonomic distinction of the reticulofenestrids (genus *Reticulofenestra*) in the Neogene (see Young, 1998, for discussion). Several research groups (Auer et al., 2019; Gibbs et al., 2005; Imai et al., 2017; Jatiningrum and Sato, 2017; Wade and Bown, 2006) apply different size ranges to differentiate *Reticulofenestra* taxa based on placolith size. We also note that each of these size ranges may contain a multitude of genotypes (Young, 1998). In this study, we follow the species concept of Auer et al. (2019) adapted for the Middle to Late Miocene:

– *Reticulofenestra* spp. (small) cf. *R. minuta*: reticulofenestrids $< 3\,\mu m$ in length without a bar spanning the central area;

– *Reticulofenestra haqii*: reticulofenestrids 3–$5\,\mu m$ in length with an open central area;

– *Reticulofenestra antarctica*: reticulofenestrids 3–$5\,\mu m$ in length with a closed central area;

– *Reticulofenestra pseudoumbilicus* (small): all reticulofenestrids 5–$7\,\mu m$ in length;

– *Reticulofenestra pseudoumbilicus* (sensu stricto): all reticulofenestrids $> 7\,\mu m$ in length.

3.2 Planktonic foraminifera counts and quantification

For foraminifera analysis, 28 samples were freeze-dried, weighed, and wet-sieved using mesh sizes of 250, 125, and $63\,\mu m$. After sieving, sample residues were oven dried at $40\,°C$. For quantitative foraminiferal analyses, the size fractions > 250 and 250–$125\,\mu m$ were examined under a stereomicroscope (Zeiss V8). In each sample, at least 200 specimens were picked and identified. In eight samples, less than 200 specimens were found in the available material. When necessary, samples were split into smaller aliquots (splits). The total number of foraminifera in the sediment ($N\,g^{-1}$) was calculated from the number of the counted specimen and the number of splits. Relative abundances (%) were calculated for each species (see Supplement S3 for details).

3.3 Statistical analyses and ordination

All applied statistical and ordination methods were performed using PAST4 (v. 4.11 released 13 September 2022; Hammer et al., 2001). The applied methods include correlation matrices between nannofossil taxa and XRF-based environmental proxy data for dust flux and Mn depletion and calcite-equivalent $CaCO_3$ content (Supplement S4), as well as the abundance of diatoms (Supplement S1). Percentage data were then arcsine-transformed before cluster analyses and ordination methods. The arcsine transformation was applied to generate a statistically viable dataset suitable for the applied clustering and ordination methods (Sokal and Rohlf, 1995; Hammer and Harper, 2006; Auer et al., 2014, 2019; Bialik et al., 2021) and utilizes the universal paired group method with arithmetic mean (UPGMA) with Bray–Curtis distance. Cluster stability was further evaluated by using UPGMA clustering with Euclidian distance and Ward's method.

The contributing taxa of each cluster were subsequently evaluated based on similarity percentage (SIMPER) analysis (Bray–Curtis similarity). The correspondence of nannofossil variability within each sample with environmental parameters was investigated using the non-metric multidimensional scaling (nMDS), where geochemical proxy data (see Sect. 2; Fig. 3) were used as environmental variables and visualized as vectors within the two-dimensional coordinate space of the nMDS. Additionally, several diversity indices (see Supplement S1), including the Shannon H' diversity, were au-

tomatically calculated for the calcareous nannofossil assemblage (Hammer and Harper, 2006).

3.4 Published geochemical proxy data used in this study

In addition to the paleobiological data generated for this study, we further use a suite of previously published geochemical proxy data (Bialik et al., 2020a), which we utilize as additional lines of evidence to anchor the observed assemblage variation within a multiproxy framework. In brief, we apply $CaCO_3$ and TOC combined with fluxes of siliceous fragments (see Sect. 3.5 for details) as productivity proxies. Benchtop X-ray fluorescence-derived elemental ratios further supplement this interpretation, where we apply Mn / Al ratios to quantify Mn redirection (see Bialik et al., 2020a) based on the model of Dickens and Owen (1994). The available XRF data were also used to generate a dust flux proxy based on the elemental ratio of $(K + Al) / (Fe + Ti + Zr)$, as defined by Kuhnt et al. (2015). This dust flux proxy allows determining the accumulation of Fe-, Ti-, and Zr-bearing heavy mineral phases compared to elements predominantly present in clay minerals $(Al + K)$. We interpret this proxy as a qualitative proxy for wind-derived dust flux and thus varying wind strength at Site 722. Dust flux and wind speed are intrinsically linked to Africa's progressive aridification due to the uplift of the Arabian Peninsula (Zhang et al., 2014; Sarr et al., 2022). The published $\delta^{15}N$ is also discussed in the context of the new assemblage data. Tripathi et al. (2017) interpret $\delta^{15}N$ values > 6‰ as an indicator for significant water column denitrification in ocean basins with oxygenated bottom waters. Later, Bialik et al. (2020a) also used this proxy interpretation for the Middle to Late Miocene interval at Site 722, which will be followed herein.

3.5 Calculation of accumulation rates and fluxes

To quantify flux rates, we applied moisture and density (MAD)-derived bulk density data generated during Leg 117 (Shipboard Scientific Party, 1989) to calculate mass accumulation rates (MAR). To calculate bulk MARs, we applied linear interpolated dry bulk density for each sample point using the calculation:

$$BMAR = \frac{DBD \times LSR}{10},$$

where BMAR is the bulk mass accumulation rate (in $g\,cm^{-2}\,kyr^{-1}$), DBD is the dry bulk density (in $g\,cm^{-3}$) based on shipboard MAD data, LSR is the linear sedimentation rate (in metres per million years) calculated based on the age model of Bialik et al. (2020a), generated bulk MARs were subsequently used to calculate mass fluxes of TOC, and $CaCO_3$ is given in $g\,cm^{-2}\,kyr^{-1}$. Fossil fluxes are given as nannofossil accumulation rates (NAR), and diatom accumulation rates (DAR) as numbers of liths and/or frustules per $cm^{-2}\,kyr^{-1}$, which are calculated by multiplying the BMAR with the number of individuals per gram of sediment.

4 Results

4.1 Calcareous nannofossils

4.1.1 Nannofossil abundance and diversity

Nannofossil preservation was good to moderately good based on visual evaluation using light and scanning electron microscopy. Overall preservation in biogenic-silica-rich samples was noted to be slightly poorer than in samples with little or no biogenic silica.

Total nannofossil fluxes range from 4.77×10^8 to 9.93×10^{10} liths $cm^{-2}\,kyr^{-1}$, with an average of 1.45×10^{10} and a median of 1.07×10^{10}. By comparison, total nannofossils per gram of dry bulk sediment range from 2.75×10^8 to 4.11×10^{10} with an average of 5.73×10^9 and a median of 4.04×10^9. Diatom accumulation ranges from no frustules to 2.41×10^{10} frustules $cm^{-2}\,kyr^{-1}$, with an average of 2.24×10^9 and a median of 3.72×10^8. In the three uppermost samples taken from Core 722B-30X, small placolith abundance (primarily *Reticulofenestra minuta*) increases sharply above the base absence (Ba) of *Reticulofenestra pseudoumbilicus* (Backman et al., 2012; Agnini et al., 2017) after 8.8 Ma (Fig. 2). For details on the abundance and variability of individual nannofossil taxa, please refer to the Supplement S2.

4.1.2 Clusters and ordination

Cluster analysis (UPGMA, Bray–Curtis similarity) resulted in four major clusters (clusters 1–4) that were defined at a similarity cutoff of 0.61 with a co-phenetic correlation coefficient of 0.81. Clusters 1 and 4 were again split into 2 (clusters 1a–b) and 3 (clusters 4a–c) sub-clusters, respectively, at a similarity cutoff of 0.66 (Fig. 4a). Bootstrapping ($N = 1000$) shows weak support for individual clusters, reflecting the overall strong similarities in the assemblage composition of the studied samples. However, one-way ANOSIM shows p values of < 0.05, indicating that the separated clusters are statistically significant.

Based on SIMPER analysis, the clusters and subclusters are primarily defined by the abundance variability of reticulofenestrids, discoasterids, *Cyclicargolithus floridanus*, and to a smaller extent *Coccolithus pelagicus*, and *Sphenolithus* spp. Based on these results, we infer that the clusters represent taphogroups, each reflecting different environmental conditions (see Auer et al., 2014).

Taphogroup (TG) 1a is characterized by a very high abundance of small reticulofenestrids. TG 1b is similarly characterized by a high abundance of small reticulofenestrids, albeit at lower levels than TG 1a, with a higher abundance of medium reticulofenestrids and *Cyclicargolithus floridanus*. TG 2 is characterized by a high abundance of *C. floridanus*, and TG 3 is characterized by a high abundance of large reticulofenestrids with common discoasterids. TG 4 and its subgroups are primarily defined by the variation in the three size
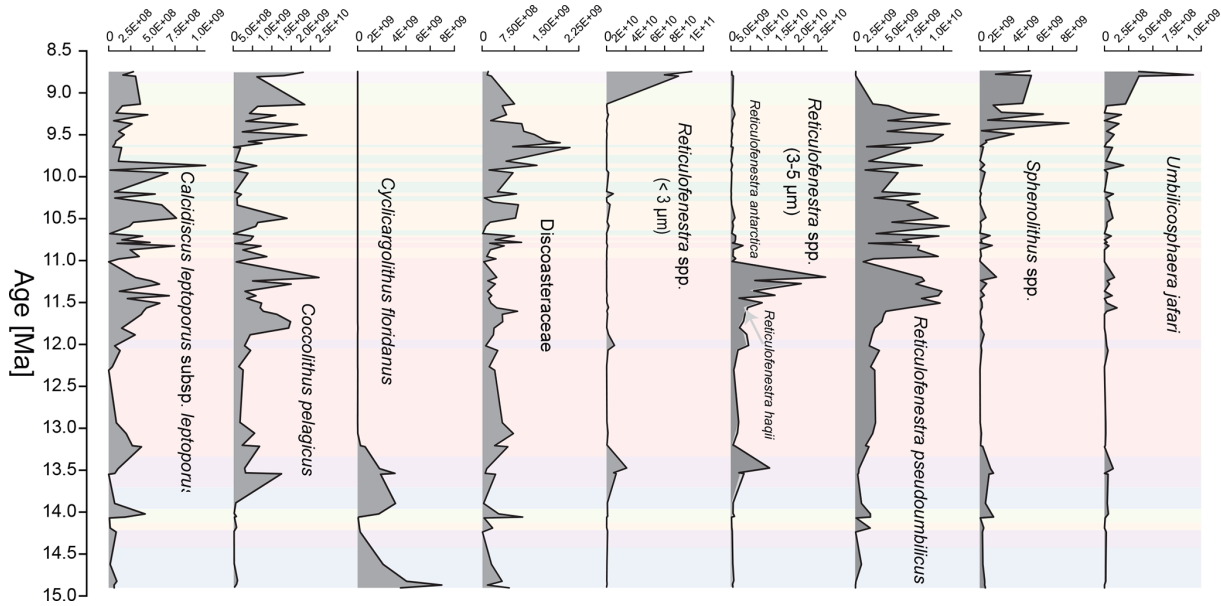
Figure 2. Nannofossils per $cm^{-2}\,kyr^{-1}$ of key nannofossil taxa over the study interval. The calculation of nannofossil abundances (per gram) used to calculate fluxes follows the method of Bordiga et al. (2015). The age model is based on Bialik et al. (2020a). Medium-sized reticulofenestrids (3–5 μm) are separated into morphotypes with an open central area (*Reticulofenestra haqii*) and a closed central area (*R. antarctica*). Discoasteraceae include the genera *Discoaster* and *Catinaster*. Colour coding represents the cluster assignment based on the nannofossil assemblage shown in Fig. 4a.
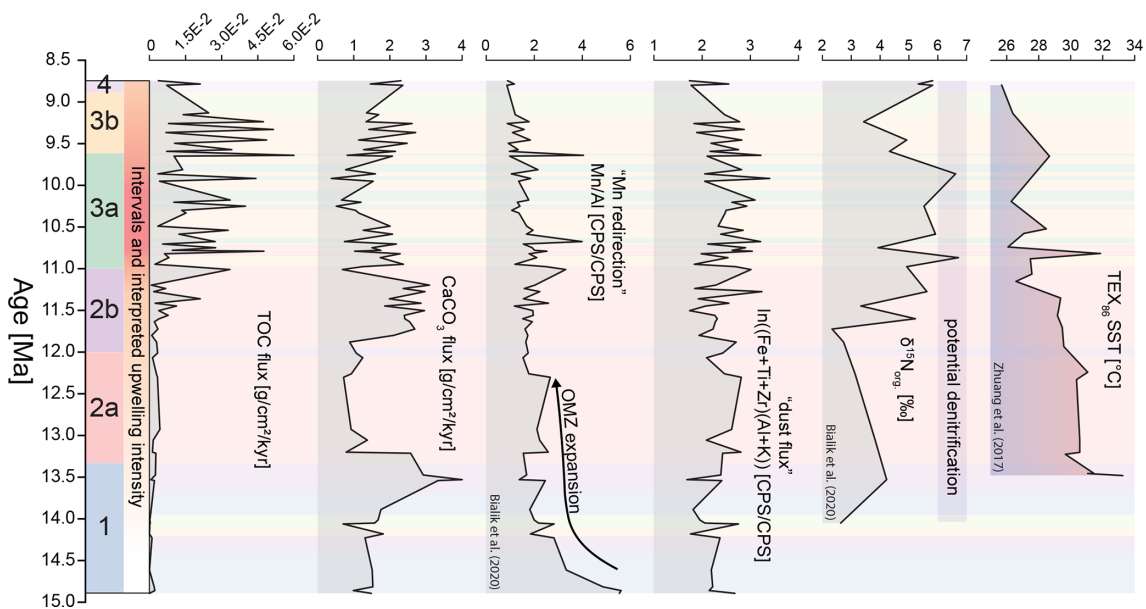
Figure 3. Geochemical data initially published by Bialik et al. (2020a) and TEX_{86}^{H}-based sea surface temperature (SST) data of Zhuang et al. (2017). Data are shown in conjunction with the cluster analysis results based on the nannofossil assemblages, as shown in Fig. 4a. Total organic carbon (TOC) and carbonate ($CaCO_3$) fluxes are based on bulk sediment analyses (see Bialik et al., 2020a). The Mn / Al ratio and the shown dust flux proxy are based on benchtop XRF counts. Dust flux is calculated as $ln((Zr + Ti + Fe) / (Al + K))$ based on Kuhnt et al. (2015), with higher values indicating higher deposition of dust-borne minerals at Site 722. Nitrogen isotopic data indicate increasing denitrification of sinking organic matter with higher values. On the left of the figure, we also show intervals 1–4, their respective sub-intervals a and b, and the resulting interpreted upwelling intensity. All data are underpinned by the assigned clusters, as defined in Fig. 4.

ranges of reticulofenestrids. Within TG 4, TG 4a exhibits the highest abundances of small reticulofenestrids, whereas TG 4b displays the lowest amounts of small and medium reticulofenestrids. Finally, TG 4c is characterized by high numbers of both medium and large reticulofenestrids. See Table 1 for a summary of the TGs and Supplement S5 for a statistical breakdown of the contribution of all taxonomic groups to each TG.

The cluster analysis results are well represented within the nMDS, with TGs splitting well along coordinates 1 and 2. Furthermore, the recorded stress of the nMDS is 0.13, indicating that the results are robust (Clarke, 1993). We, however, note the overall high compositional similarity of clusters, particularly sub-clusters, which results in higher stress in the nMDS. This is important, as recently a more conservative approach has been put forward, recommending that nMDS outputs exhibiting stress above 0.1 should be carefully evaluated (Bialik et al., 2021). We found a positive loading for TOC and diatoms along coordinates one and two. Dustflux, calculated as $\ln((\mathrm{Zr} + \mathrm{Ti} + \mathrm{Fe}) / (\mathrm{Al} + \mathrm{K}))$ following Kuhnt et al. (2015), is positively loaded on coordinate one but negatively loaded on coordinate two. The Mn / Al ratio is loaded negatively on coordinate 1 and positively on coordinate 2, whereas $CaCO_3$ is loaded negatively on both coordinates (Fig. 4b).

4.2 Planktonic foraminifera

Out of 28 samples, 1 sample (722B-34X-3W 30-32, ca. 10.2 Ma) was barren in planktonic foraminifera. In the remaining 27 samples, 27 taxa of planktonic foraminifera were identified (Supplement S3). The planktonic foraminifera preservation was overall good but decreases downhole. The foraminifera tests were found to be moderately pyritized. Of these taxa, five (*Globigerinoides ruber*, *Globorotalia menardii*, *Neogloboquadrina acostaensis*, *Paragloborotalia mayeri*) have their stratigraphic first or last occurrence within the studied interval. All recorded taxa were grouped according to their environmental preferences following established environmental assignments of either mixed-layer taxa, open-ocean thermocline taxa, open-ocean sub-thermocline taxa, upwelling taxa, or unknown (Table 2).

Through the studied interval, thermocline species and mixed-layer taxa are the most abundant (abundance reaches more than 50 %). Both mixed-layer and upwelling taxa increase in prevalence through the studied interval, while thermocline species decrease. A sharp drop in thermocline taxa occurs between 11 and 10 Ma, corresponding to the disappearance of *Paragloborotalia mayeri*, the dominant taxa until that time. Mixed-layer taxa remain at a near-stable level from 11 Ma onwards. Upwelling taxa are not represented in two samples between 11 and 10.8 Ma, after which this group exhibits a steady increase until the end of the studied interval. Sub-thermocline taxa are present between 9.0 and 9.5 Ma

and account for only a small fraction (less than 3 % at most) of the assemblage.

5 Discussion

5.1 Definition of taphogroups and their paleoenvironmental significance

Based on the above results, we interpret the analysed samples in the context of their taphogroups. Taphogroups represent the total preserved fossil assemblage deposited at a given time in the past. Therefore, samples assigned to contain the same taphogroup can be assumed to reflect similar local surface water conditions at Site 722.

Taphogroup 1a. TG1a is dominated by small reticulofenestrids. We therefore interpreted this TG as indicative of high nutrient levels, facilitating the proliferation of small bloom-forming placoliths (primarily *Reticulofenestra minuta*; see Table 1, Supplement S5). Small reticulofenestrids are commonly associated with high terrigenous nutrients in near-shore environments (see references in Table 1). However, as Site 722 was located in the open ocean throughout the study interval (Bialik et al., 2020a), changes in terrigenous nutrient sources are unlikely, and a different mechanism must be invoked for this dominance of small reticulofenestrids. Studies based on coccolithophore cultures indicate that the proliferation of small placoliths may result from nitrogen limitation in a highly productive open marine environment. For example, Paasche (1998) showed that modern-day coccolithophores tend to increase the formation of small placoliths during N limitation. Hence, we assume that the proliferation of small reticulofenestrids in the open-ocean results from increasing nitrogen limitation compared to other macro- or micronutrients. Such N-limited environments often persist in settings with high productivity due to rapid N-loss during denitrification (Paerl, 2018), which would fit with the above interpretation of small reticulofenestrid proliferation at Site 722, offshore Oman.

Taphogroup 1b. The presence of common *C. floridanus* in combination with abundant small- and medium-sized reticulofenestrids within this assemblage indicates elevated nutrient levels compared to a fully oligotrophic assemblage (see Table 1 and Supplement S5). The very high but not dominant abundance of small reticulofenestrids may also point to N-limited nutrient sources (see TG 1a). This will be analogous to the fringes of the modern-day Arabian Sea upwelling cell, where nitrogen may be the primary limiting nutrient (Anju et al., 2020), hinting at the presence of upwelling during TG1b, which was more confined to the coast of the Arabian Peninsula and did not fully reach Site 722. Compared to other TGs, the overall high diversity suggests intermittent (likely seasonal) oligotrophic conditions, which may also point towards phosphate co-limitation when upwelling is limited. We thus interpret TG 1b as reflective of open marine conditions with only somewhat elevated nutrient levels compared to an open-

Table 1. Ecological interpretation of the defined nannofossil taphogroups based on the ecological parameters of the defining nannofossil taxa.

Taphogroup	Defining taxa	Ecology	References	Environmental parameters
TG 1a	Reticulofenestra minuta dominant	Dominated by r-selected opportunistic nannofossil taxa. Commonly interpreted as nutrient elevation in the photic zone.	Haq (1980); Wade and Bown (2006); Auer et al. (2015)	Associated with high calcium carbonate accumulation
TG 1b	Small and medium reticulofenestrids together with Cyclicargolithus floridanus	Warm to temperate waters with increased nutrient conditions.	Wei and Wise (1990); Wade and Bown (2006); Auer et al. (2015)	Associated with high calcium carbonate accumulation
TG 2	Cyclicargolithus floridanus and common medium reticulofenestrids	Warm to temperate waters with moderate nutrient conditions.	Wei and Wise (1990); Wade and Bown (2006); Auer et al. (2015)	Associated with high Mn / Al ratios (weak OMZ) and elevated carbonate content
TG 3	Large reticulofenetrids dominant with common discoasterids	Elevated nutrient conditions with deep nutricline and possible (seasonal) stratification	Lohmann and Carlson (1981); Backman et al. (2013); Imai et al. (2015, 2017)	Associated with biogenic silica, TOC, dust flux and lowered Mn / Al ratios (stronger OMZ)
TG 4a	Variable small, medium, and large reticulofenestrids with common Sphenolithus spp. and discoasterids	Elevated nutrient conditions with high seasonal variability and intermittent stratification. Possible indication of increased environmental stress.	Castradori (1998); Blanc-Valleron et al. (2002); S. J. Gibbs et al. (2004); Wade and Bown (2006); Villa et al. (2008); Beltran et al. (2014); Imai et al. (2015); Schueth and Bralower (2015)	Weakly associated with carbonate accumulation and higher Mn / Al ratios (weak OMZ)
TG 4b	Large reticulofenestrids dominant	High nutrient conditions, likely open marine and potentially stratified.	Auer et al. (2014, 2015); Beltran et al. (2014); Imai et al. (2017, 2015)	Weakly associated with biogenic silica flux, TOC, and reduced Mn / Al ratios (increasing OMZ)
TG 4c	Medium and large reticulofenestrids dominant	High nutrient levels, likely upwelling derived.	Haq and Lohmann (1976); Lohmann and Carlson (1981); Wade and Bown (2006); Auer et al. (2014, 2019)	Not associated with Mn / Al ratios (strong OMZ); no strong association with other parameters

ocean gyre. Primary nutrient supply, however, is still controlled by nutrients derived through the remineralization of locally produced particulate organic matter (Cullen, 1991), likely supplied to the surface water through seasonal mixing during weaker summer monsoons.

Taphogroup 2. Within TG 2, common *C. floridanus* occurs together with medium and large reticulofenestrids, commonly associated with warmer water temperature, a deep nutricline, and potentially elevated nutrient conditions (Table 1 and Supplement S5). Therefore, we interpret this TG to reflect open marine conditions without directly indicating upwelling-derived nutrients. Nutrients were likely mainly derived through particulate organic matter remineralization, with low external nutrient influx through upwelling or terrigenous nutrients.

Taphogroup 3. Previous studies (Auer et al., 2014; Lohmann and Carlson, 1981) generally associated large reticulofenestrids with high nutrient conditions. Imai (2015) states that dominant large reticulofenestrids and common discoasterids indicate low nutrient conditions and a deep nutricline compared to a high abundance of small reticulofenestrids (Table 1 and Supplement S5). However, this interpretation is questioned by the association of TG 3 with high TOC, high dust flux, and high silica accumulation rates, indicating strong upwelling conditions (Fig. 4b). Although, similar co-occurrences of diatoms and discoasterids were previously recorded in the eastern equatorial Pacific and the Mediterranean (Backman et al., 2013).

While difficult to ascertain, the association of TG 3 with high dust flux and thus additional iron fertilization may rep-

Table 2. Interpretation of habitat depth of the identified planktonic foraminifera taxa.

| Taxa	Habitat	Reference	Comments
Dentoglobigerina altispira	open-ocean mixed layer	Berggren et al. (1985); Aze et al. (2011)	Symbiont bearing
Fohsella fohsi	open-ocean thermocline	Aze et al. (2011)	
Fohsella peripheroronda	open-ocean thermocline	Berggren et al. (1985); Aze et al. (2011)	Extends to cool subtropical waters
Globigerina bulloides	upwelling	Kroon et al. (1991)	
Globigerina sp.	open-ocean mixed layer	Aze et al. (2011)	
Globigerinita glutinata	open-ocean mixed layer	Majewski (2003); Pearson and Wade (2009)	
Globigerinoides obliquus	open-ocean mixed layer	Nikolaev et al. (1998)	
Globigerinoides ruber	open-ocean mixed layer	Nikolaev et al. (1998)	Symbiont bearing
Globigerinoides sp.	open-ocean mixed layer		Based on other present taxa of this genus
Globoquadrina dehiscens	open-ocean thermocline	Pearson and Shackleton (1995); Nikolaev et al. (1998)	Noted to be erratic and variable by Pearson and Shackleton (1995)
Globorotalia archaeomenardii	open-ocean thermocline		Based on similarities to *G. menardii*
Globorotalia menardii	open-ocean thermocline	Regenberg et al. (2010)	
Globorotalia plesiotumida	open-ocean thermocline	Aze et al. (2011)	
Globorotalia scitula	open-ocean sub-thermocline	Itou et al. (2001)	*G. scitula* flux is inverse to particulate organic carbon flux
Globorotalia sp.	open-ocean thermocline		Based on other present taxa of this genus
Globorotaloides hexagonus	upwelling	Spezzaferri (1995)	May also be a deep sub-thermocline dweller (Brummer and Kučera, 2022)
Globoturborotalita druryi	open-ocean mixed layer	Kennett and Srinivasan (1983); Aze et al. (2011)	Symbiont bearing
Globoturborotalita nepenthes	open-ocean mixed layer	Aze et al. (2011)	
Neogloboquadrina acostaensis	open-ocean thermocline	Aze et al. (2011)	
Orbulina universa	open-ocean mixed layer	Aze et al. (2011)	
Paragloborotalia mayeri	open-ocean thermocline	Aze et al. (2011)	
Sphaeroidinellopsis seminulina	open-ocean thermocline	Aze et al. (2011)	
Sphaeroidinellopsis sp.	open-ocean thermocline	Aze et al. (2011)	
Trilobatus quadrilobatus	open-ocean mixed layer	Chaisson and Ravelo (1997)	Deep mixed layer in Nikolaev et al. (1998)
Trilobatus sacculifer	open-ocean mixed layer	Aze et al. (2011)	Symbiont bearing
Trilobatus trilobus	open-ocean mixed layer	Aze et al. (2011)	Symbiont bearing
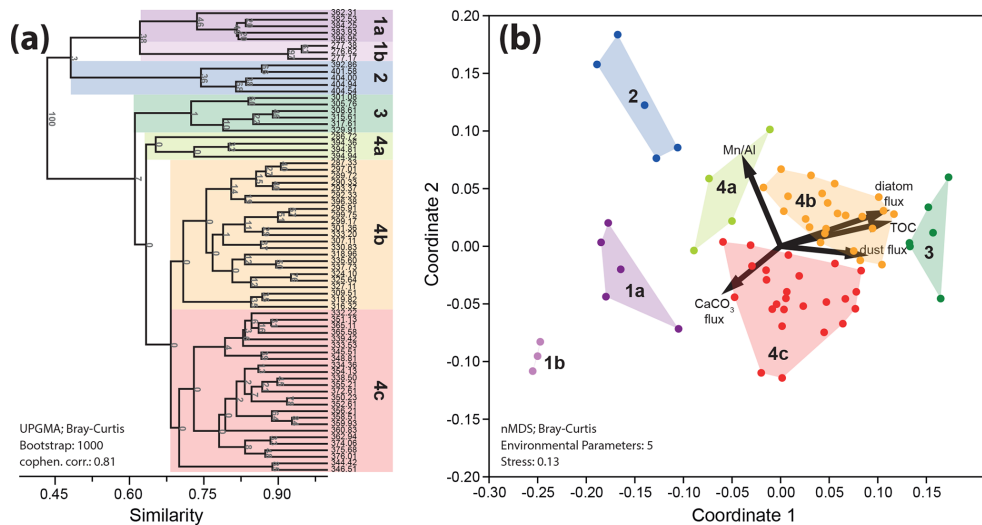
Figure 4. Cluster analysis **(a)** and nMDS **(b)** based on the datasets shown in Figs. 2 and 3. The geochemical data serve as paleoenvironmental proxies for high productivity (total organic carbon and diatom fluxes), high wind intensity (dust flux), water column oxygenation (Mn / Al), and high carbonate accumulation (CaCO$_3$ flux). Note the high correspondence of clusters 3 and, to some degree, 4b diatom accumulation, dust flux, and high TOC content. They indicate that these clusters likely correspond to nannofossil assemblages thriving during intense upwelling. Conversely, lower productivity and thus higher water column oxygenation are marked by a correspondence of clusters 2 and 4a with higher Mn / Al values, denoting a less intense oxygen minimum zone.

resent exceptionally high primary productivity (Guieu et al., 2019). Furthermore, modern analogues based on large *Geophyrocapsa* taxa, descendants of the genus *Reticulofenestra* (Samtleben, 1980; Perch-Nielsen, 1985; Nannotax 3, 2023), are more abundant in high nutrient upwelling zones (Bollmann, 1997). However, seasonality between summer monsoon and weak or absent winter monsoon could also address this discrepancy in the interpretation of TG 3 with available environmental data. Diatom and coccolithophore accumulation occur in such a setting in different nutrient regimes. Modern-day culture studies of coccolithophores (Paasche, 1998) also show that the calcification of coccolithophores increases during nitrogen excess and phosphate limitation.

Therefore, we interpret TG 3 as indicative of likely the strongest summer monsoon-controlled upwelling for our Middle to Late Miocene study interval. Conversely, a relatively weak winter monsoon resulted in a deep nutricline for the rest of the year.

Taphogroup 4a. Taphogroup 4a is not dominated by a specific reticulofenestrid size range while also containing a diverse assemblage in general (see Table 1). We therefore interpret this TG to show weaker upwelling conditions compared to TG3 or TG 1a during transient climatic conditions. Furthermore, weaker productivity is implied by a stronger association of TG 4a with higher Mn / Al values (Fig. 4b).

Taphogroup 4b. The high dominance of large reticulofenestrids of TG 4b would suggest elevated, upwelling-derived nutrient levels in a temperate upwelling zone (see TG3 above). Furthermore, the level of calcification rates, as found in experimental studies by Paasche (1998), may also indi-

cate *P*-limitation. High nutrient conditions are corroborated by the general association of TG 4b with high diatom fluxes, TOC, and dust flux in the nMDS (Fig. 4b).

Taphogroup 4c. Taphogroup 4c is defined by both medium and large reticulofenestrids (Table 1, Supplement S5). Therefore, we interpret this TG as indicative of weaker but sustained upwelling conditions. In addition, it shows some association with upwelling indicators such as dust flux and no association with the Mn / Al ratio in the sediment (Fig. 4b), indicating that it is only associated with an overall active upwelling zone and active Mn redirection and therefore OMZ conditions at Site 722.

5.2 Temporal progression of environmental changes

Individual taphogroups represent specific eco-spaces, but to understand the relation and transitions between these eco-spaces in their temporal context, their variability must be considered in relation to other proxies within a multi-proxy approach. Integrating the analyses of nannofossil taphogroups (Table 1), planktonic foraminifera data (Fig. 5), and the abundance of diatom fluxes and geochemical data (Bialik et al., 2020a), we delineate temporal intervals in Site 722. These reflect stratigraphic intervals of specific environmental conditions in the WAS.

Interval 1 (base of study interval–13.4 Ma). This interval is characterized by variable taphogroups belonging to TG 1a, TG 2, TG 4a, and TG 4b. The variable taphogroups reflect a diverse and variable nannofloral assemblage in this interval. Overall, the nannofloral assemblages are charac-
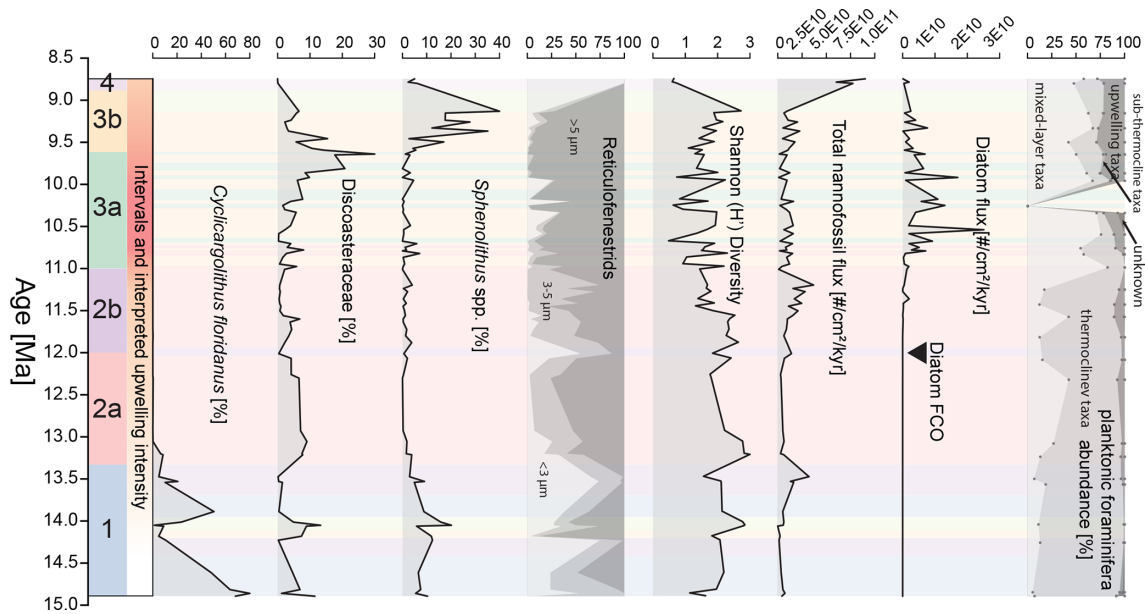
Figure 5. Summary of relevant nannofossil taxa (*C. floridanus*, the sum of all Discoasteraceae, *Sphenolithus* spp., and all three selected size ranges of *Reticulofenestra* spp.) shown as percentage abundance of the whole assemblage. Reticulofenestrids are combined into a single abundance graph showing the internal variability of the three defined size ranges of the genus *Reticulofenestra*. The Shannon (H') diversity is offered as an overall indicator of nannoplankton diversity throughout the study interval. The total abundance of nannofossil fluxes in individuals per $cm^{-2} kyr^{-1}$ illustrates the stark increase in nannofossil accumulation in interval 4, denoting the noted bloom in small reticulofenestrids after 8.8 Ma. Next, the nannofossil abundances are contrasted with diatom fluxes. The nannofossil assemblage variability is further shown with classical upwelling indicators based on planktonic foraminifera, which show an overall constant abundance of upwelling indicative taxa (e.g. *G. bulloides*) between intervals 3a and 4, despite the dynamic changes in the phytoplankton data. On the left of the figure, we also show intervals 1–4, their respective sub-intervals a and b, and the resulting interpreted upwelling intensity. All data are underpinned by the assigned clusters, as defined in Fig. 4.

terized by a high abundance of *Cyclicargolithus floridanus* (Fig. 5). However, *Cyclicargolithus floridanus* abundances decline through the interval to its stratigraphic Top (T) occurrence at Site 722. In addition, we record abundant small reticulofenestrids and peaks of discoasterids (TG 4a, 4b). The average number of taxa in interval 1 is 14.9 ± 2.1 ($N = 13$), with an average Shannon H' diversity of 1.6 ± 0.4. The planktonic foraminifera assemblage is dominated by thermocline-dwelling taxa (predominantly *P. mayeri*). Siliceous fragments are absent. We interpret this interval as a relatively low nutrient environment based on the above multi-group assemblage composition. In particular, the presence of TG 1a and 2 points to only moderately elevated nutrient concentrations in the surface waters at Site 722 during the MMCT. The common occurrence of *Sphenolithus* spp. and discoasterids suggests seasonally intermittent stratification. These results are consistent with the relatively warm SSTs recorded during this interval (Zhuang et al., 2017), further supporting a generally muted upwelling regime in the WAS during interval 1. These assumptions are corroborated by a more limited OMZ extent in the Indian Ocean compared to the later Miocene. At Site 722 this is shown declining Mn content. On the Maldives, high Mn concentrations and the absence of notable drift deposits, and thus lower wind intensity, also

corroborate a generally weaker OMZ during this time (Bialik et al., 2020b; Betzler et al., 2016).

Interval 2a (13.4–12.0 Ma). Interval 2a is solely comprised by TG 4c. This taphogroup is characterized by a diverse assemblage with abundant *R. pseudoumbilicus* and common medium-sized reticulofenestrids and discoasterids. The average number of taxa is 16.6 ± 2.2 ($N = 7$), with an average Shannon H' index of 1.8 ± 0.3. Siliceous fragments are absent. Planktonic foraminiferal assemblages are dominated by thermocline species with increased abundances of mixed-layer species compared to interval 1. Within interval 2a, a first slight increase in upwelling indicative taxa (primarily *G. bulloides*) is observed (Fig. 5). We interpret this interval as indicative of a first shallowing of the thermocline due to the initial strengthening of the wind-driven upwelling regime at Site 722. This intensification is likely related to an intensification of the monsoon system following the end of the MMCT (Betzler et al., 2018). The intensification of the monsoon system is also consistent with the establishment of an increased OMZ extent and drift deposits in the Maldives (Betzler et al., 2016).

Interval 2b (12.0–11.0 Ma). Interval 2b is comprised primarily of assemblages belonging to TG 4c, with one sample belonging to cluster 1b. The interval similar to interval

2a is characterized by assemblages (TG 4c) with abundant medium-sized reticulofenestrids that occur together with an increase in large reticulofenestrids (Figs. 2, 5). Furthermore, we detect a small but noteworthy increase in *Umbilicosphaera jafari* and a decline in Discoasteraceae. Moreover, the abundance of small reticulofenestrids is lower than in interval 2a. These differences within the assemblage are also the reason why interval 2 was separated into the two sub-intervals. The average number of taxa in interval 2b is 15.6 ± 2.6 ($N = 16$), with an average Shannon H' index of 1.5 ± 0.3. The base of interval 2b also contains the first occurrence of diatoms within the section. Planktonic foraminifera mixed layer taxa decrease while upwelling taxa increase further in this interval.

We interpret this interval to mark a progressive intensification in the upwelling of high-nutrient subsurface waters. We base this on (1) the increase in siliceous fragments (diatoms and other siliceous biota, (2) higher abundances of upwelling indicative planktonic foraminiferal taxa, and (3) generally nutrient-adapted nannofossil taxa (i.e. medium- and large-sized reticulofenestrids; Beltran et al., 2014; Auer et al., 2015; Imai et al., 2015), which show progressive abundance increases. Intensified upwelling is consistent with increasing $\delta^{15}N$ values and continuous cooling at Site 722 (Zhuang et al., 2017; Bialik et al., 2020a). Increased upwelling-derived nutrient access in the northern Indian Ocean is further supported by increased productivity and nitrogen utilization in the Maldives (Betzler et al., 2016; Ling et al., 2021). The upwelling intensification after 12 Ma is consistent with an overall increase in global atmospheric circulation and oceanic current strength, including the Indian Ocean South Equatorial Current (Fig. 6; House et al., 1991; Gourlan et al., 2008; Groeneveld et al., 2017; Betzler and Eberli, 2019).

Interval 3a (11.0–9.6 Ma). Interval 3a is characterized by a dominance of large reticulofenestrids (*R. pseudoumbilicus*) (TG 3) with intermittently common discoasterids and small reticulofenestrids (TG 4b). Notably, medium-sized reticulofenestrids show very low abundances compared to the previous intervals (Fig. 5). The abundance of *Umbilicosphaera jafari* is highly variable but overall common. At the same time, sphenoliths are rare in the lower part of the interval before increasing (up to $\sim 40\%$ of the assemblage) in the upper part. Within this interval, we also note the occurrence of variable abundances of small reticulofenestrids between ~ 10.5 to 9.9 Ma. The average number of taxa is 14.3 ± 5.1 ($N = 22$), with an average Shannon H' index of 1.1 ± 0.4. The high environmental variability within this interval is illustrated by alternations between assemblages belonging to TG 3, 4b, and 4c. Diatom fluxes increase significantly (Fig. 5). Diatoms generally dominate the phytoplankton assemblage, even outcompeting calcareous nannoplankton in terms of total abundance. High diatom abundances are especially prevalent within samples assigned to TG 3. Mixed-layer taxa dominate planktonic foraminifera assemblages and increase in this interval, together with upwelling

taxa. Notably, thermocline species decline to less than half of their previous abundance. One sample (722B-34X-3W 30-32) is barren of planktonic foraminifers. The lack of foraminifera is likely due to the limited sample amounts washed for this study, in conjunction with the high accumulation rates of phytoplankton (diatoms and calcareous nannofossils) in this stratigraphic interval.

Based on the high abundance of diatoms and a generally high nutrient-adapted nannofossil assemblage, we interpret interval 3a as a peak in upwelling intensity at Site 722. This interpretation is consistent with previously published $\delta^{15}N$ data from Site 722, sites U1466 and U1468, and other geochemical datasets in the Maldives (Bialik et al., 2020a; Ling et al., 2021). In addition, high productivity and OMZ expansion are further recorded by heightened TOC, uranium accumulation, and low Mn deposition within the northwestern Indian Ocean (Dickens and Owen, 1994, 1999; Betzler et al., 2016; Bialik et al., 2020a). This corresponds to an increase in Antarctic Bottom Water (AABW) formation due to the expansion of North Atlantic Deep Water (NADW), indicative of an intensified global thermohaline circulation (Woodruff and Savin, 1989). Increasing numbers of discoasterids in the upper part of interval 3a and decreasing diatoms numbers also point towards declining upwelling and thus seasonal nutrient depletion when no summer monsoon-derived upwelling occurs. This pattern of clear seasonality imparted on the plankton flux further amplifies within the next interval.

Interval 3b (9.6–8.8 Ma). Interval 3b continues to exhibit a dominance of large reticulofenestrids (*R. pseudoumbilicus*) (TG 3), although discoasterids noticeably decline and are replaced by higher abundances of sphenoliths (primarily *Sphenolithus moriformis*), with abundances of $\sim 40\%$ of the total assemblage. Small- and medium-sized reticulofenestrids are rare in this interval (Figs. 2, 5). The average number of taxa is 15 ± 2.3 ($N = 10$), with an average Shannon H' index of 1.4 ± 0.3.

We thus interpret interval 3b to indicate decreasing upwelling intensity based on the increase in nannofossil taxa adapted to warmer and more stratified water masses, such as *Discoaster* spp. and *Sphenolithus* spp. (Lohmann and Carlson, 1981; Castradori, 1998; Negri and Villa, 2000; Blanc-Valleron et al., 2002; Gibbs et al., 2004a; Aubry, 2007; Villa et al., 2008; Schueth and Bralower, 2015). The waning upwelling of the northern Indian Ocean is corroborated by the proliferation of warm-water diatom taxa in the Maldives (Site 714; Boersma and Mikkelsen, 1990). Decreasing $\delta^{15}N$ values support waning upwelling-derived productivity after 10 Ma at both Site 722 and in the Maldives and decreasing TOC fluxes at Site 722 (Gupta et al., 2015; Bialik et al., 2020a; Ling et al., 2021). It is, however, important to note that these changes are not reflected in the planktonic foraminifera community, which shows a continuously high presence of upwelling taxa (e.g. *G. bulloides*). One possibility would be that the upwelling cell became more seasonal,
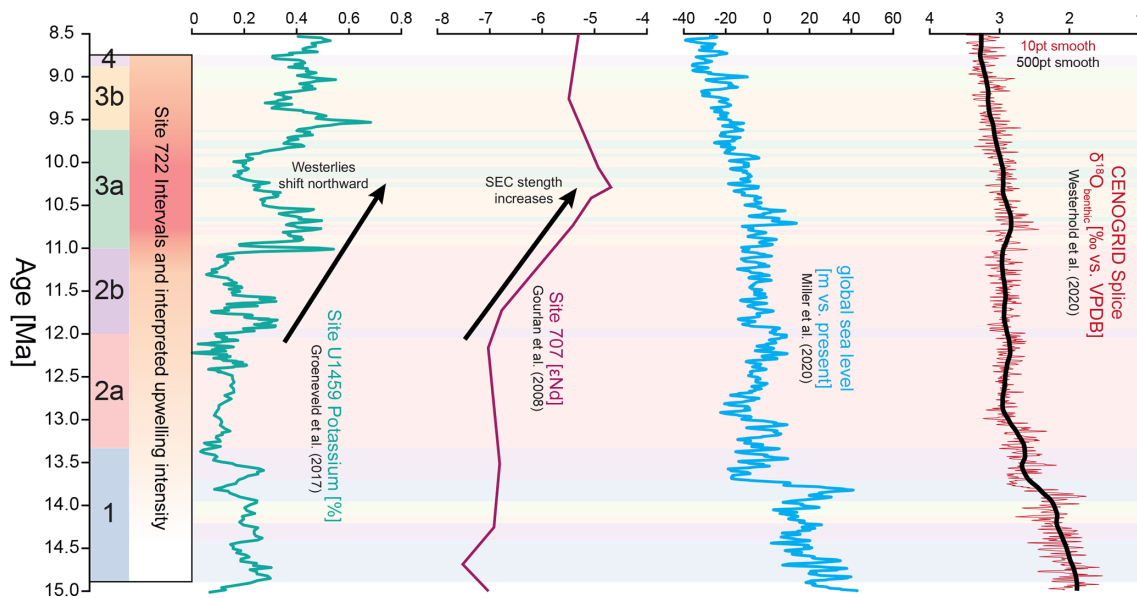
Figure 6. Compilation of Indian Ocean and global data during the study interval. Proposed plankton community intervals, as well as nannofossil assemblages at Site 772, are presented next to the abundance of natural gamma-radiation-derived potassium content at Site U1459 (Groeneveld et al., 2017), interpreted to relate to precipitation changes in Western Australia as a consequence of the northward-shifting Southern Hemisphere westerlies. The εNd data of Gourlan et al. (2008) show an increase in εNd signatures derived from Indonesia, indicating an increase in SEC strength due to a global increase in global ocean and atmospheric circulation (e.g. Betzler and Eberli, 2019). Conversely, the global sea level reconstruction of Miller et al. (2020) indicates stable sea levels after the MMCT until at least 11 Ma. The global CENOGRID stable oxygen isotope stack also shows stable deep-water conditions and ice volume until 11 Ma (Westerhold et al., 2020). On the left of the figure, we also show intervals 1–4, their respective sub-intervals a and b, and the resulting interpreted upwelling intensity. All data are underpinned by the assigned clusters, as defined in Fig. 4.

with nannoplankton-dominated photoautotrophic communities proliferating seasons with lower upwelling. However, primarily heterotrophic, non-symbiont-bearing taxa such as *G. bulloides* were still sustained by high primary productivity during monsoon season, as is the case in the present-day upwelling cell along the Oman margin (Schiebel et al., 2004; Rixen et al., 2019b).

We assume that this waning in upwelling is related to a decrease in the hemispheric temperature gradients, leading to a weaker summer monsoon wind system in the Indian Ocean. This reduction in temperature gradients is consistent with a decreasing trend in minimum deep-water temperatures, based on global benthic foraminifera compilations and deep-water records from the Ninety East Ridge (Site U1443; Fig. 1) (Lübbers et al., 2019; Westerhold et al., 2020). Furthermore, pollen data (Pound et al., 2012) suggest that progressive cooling of the Northern Hemisphere (NH) over the Middle to Late Miocene intensified. Northern Hemisphere cooling consequently reduced the asymmetry of hemispheric temperature gradients, thereby reducing summer monsoon wind intensity by muted northward migration of the intertropical convergence zone (ITCZ) in NH summer (Gadgil, 2018; Yao et al., 2023).

Interval 4 (8.8 Ma–top of study interval). Interval 4 – consisting of only three samples – is defined by the bloom of

small reticulofenestrids (*R. minuta*) in the nannofossil assemblage. We also note an elevated abundance of *Umbilicosphaera jafari* and a marked decline in *Sphenolithus* spp. relative to interval 3b. This interval consists entirely of assemblages belonging to TG 1b (Figs. 2, 5). The average number of taxa is 17.3 ± 0.5 ($N = 3$), with an average Shannon H' index of 0.5 ± 0.0. Despite the high number of nannofossil taxa in this interval, the low diversity directly results from the dominance of small reticulofenestrids. Siliceous fragments (primarily diatoms) persist but are much rarer than in interval 3. This reduction in diatom fluxes is part of an ongoing decrease in biogenic silica accumulation at Site 722, which culminates in a shift from phytoplankton- to zooplankton-dominated silica accumulation by ~ 8 Ma (Nigrini, 1991; Prell et al., 1992). Planktonic foraminifera assemblages remain consistent with the upper part of interval 3, showing relatively high abundances of upwelling and mixed-layer taxa. We interpret this interval as a new nutrient regime, which likely led to a significant turnover in coccolithophore species around the same time (Young, 1990; Imai et al., 2015). However, the low sample number in this interval limits further interpretation.

5.3 Plankton community responses to paleoenvironmental changes

Based on the intervals defined by the nannofossil taphogroups, a progression of plankton communities becomes apparent within the Middle to Late Miocene at Site 722. Their variation highlights the strong interactions between monsoon wind strength, nutrient availability, and primary productivity. Therefore, we link our new assemblage data with previous regional publications, highlighting a progressive upwelling increase leading to thermocline shoaling (Fig. 3; Zhuang et al., 2017; Bialik et al., 2020a). This thermocline shoaling in turn results in declining sea surface temperatures and increased surface water productivity through the upwelling of nutrient-rich thermocline waters along the Oman margin during this time.

Declining high Mn / Al ratios and diverse nannofossil assemblages point towards a relatively low nutrient regime between 15.0 and 13.5 Ma. Patterns of Mn decline have been observed since at least 15 Ma in the Maldives, which is in line with observations at Site 722 (Betzler et al., 2016, 2020a, b). This period thus represents a progressive increase in upwelling intensity during the MMCT due to globally declining SSTs and sea levels following the end of the MCO (Zhuang et al., 2017; Miller et al., 2020). Both nannoplankton and planktonic foraminifera reflect primarily open marine, low-nutrient conditions (Sexton and Norris, 2011; Lessa et al., 2020).

By 13.5 Ma, these progressive changes culminate in a first sustained community shift in nannofossil and planktonic foraminifera records (Figs. 2, 5). We consider these shifts to be a coupled response of Site 722 phytoplankton communities to increased surface water nutrient levels that subsequently allowed a population increase of heterotrophs such as foraminifera. These changes are consistent with establishing a more pronounced upwelling regime, which also resulted in the expansion of the OMZ further into the Indian Ocean, reaching the Maldives by ∼ 13 Ma. Furthermore, available TOC data still show low accumulation rates at Site 722 at this time, indicating that organic matter was still recycled mainly within the expanding OMZ (Bialik et al., 2020a).

By ∼ 12 Ma, another phytoplankton community shift (see interval 2b) leads to a size increase in the reticulofenestrids, lower nannoplankton diversity, and a higher abundance of thermocline-dwelling planktonic foraminifer taxa (Fig. 5). Together with increasing TOC fluxes (Fig. 3), all of these shifts point towards increasing productivity. These changes, however, happen without any significant changes in overall temperature within the upwelling zone (Zhuang et al., 2017). A northward shift in the Southern Hemisphere westerlies is recorded by 12 Ma (Groeneveld et al., 2017). We hypothesize that this shift and a potential increase in wind strength may have also increased nutrient concentrations in intermediate water masses within the sub-Antarctic frontal system. This interpretation would be in line with the effect increas-

ing sea ice cover would have had on intermediate water nutrient concentrations based on modelling data and evidence from Southern Hemisphere records (Sarmiento et al., 2004; Sarmiento, 2006; Laufkötter and Gruber, 2018; Groeneveld et al., 2017). Such enhanced nutrient transport within the thermocline would reconcile increased productivity without increasing the total volume of upwelling – and consequently reducing SSTs – along the Oman margin. The first occurrence of diatoms within this interval may also point towards a shift in nutrient availability and increased phosphorus and silicon availability within the upwelling cell and likely globally (Keller and Barron, 1983). Decreasing P and Si limitation would thus provide more favourable conditions for highly efficient photosynthesizers, such as diatoms within the water column (Schiebel et al., 2004; Brembu et al., 2017; Sarmiento, 2006). Within the plankton community, we also note the first intermittent occurrences of elevated *G. bulloides* abundances, indicative of high-productivity upwelling conditions (Kroon et al., 1991; Gupta et al., 2015).

By 11 Ma, global climatic shifts and further decreasing sea levels (Miller et al., 2020; Westerhold et al., 2020) led to another step in the water masses upwelling in the WAS (Fig. 6). As a result of these water mass changes, diatoms dominate our phytoplankton record by 11 Ma, outpacing nannoplankton for the first time, while we note a first sustained occurrence (> 25 %) of *G. bulloides*. Therefore, we interpret this shift as the inception of sustained primary productivity within the upper water column of an upwelling cell supplied with enough Si, as well as P and N, to sustain a large diatom population (Brzezinski, 1985; Sarmiento, 2006; Closset et al., 2021).

However, the abundance of discoasterids and spheno-liths within our nannofossil record (Fig. 5) still needs to be reconciled with this interpretation. Both taxa are considered to be indicative of low nutrient conditions and increased stratification (Gibbs et al., 2004a; Schueth and Bralower, 2015; Karatsolis and Henderiks, 2023). This information is thus contrary to our recorded high abundances of mixed-layer-dwelling foraminifera and high-nutrient-adapted diatoms dominating the phytoplankton record. A possible way of integrating these opposite requirements is to evoke a highly seasonal upwelling cell with strong upwelling in one season and calm and stratified surface waters providing a deep thermocline and nutricline in the other.

This seasonal variability is most evident after 9.6 Ma when *Sphenolithus* abundances also increase together with overall nannofossil diversity (Fig. 5, interval 3b). These changes in the nannofossil community are also associated with decreasing diatom abundances and TOC fluxes, while upwelling indicative planktonic foraminifera taxa remain common. It thus seems that an initial spike in upwelling and therefore diatom accumulation waned again, pointing towards a significant reorganization of the upwelling cell after 9.6 Ma.

Within the topmost three samples of the record, belonging to interval 4, we note an increase in small reticulofen-

estrids corresponding to the base absence of *Reticulofenes-tra pseudoumbilicus* around 8.8 Ma, according to accepted nannofossil biostratigraphy (Young, 1990; Backman et al., 2012; Imai et al., 2015). We note that this significant size change and an increase in small placoliths are very pronounced within our WAS records from Site 722, in agreement with Young (1990). While we cannot contribute to the discussion of whether this assemblage shift constitutes an evolutionary-driven adaptation of taxa within the genus *Reticulofenestra* or purely an ecophenotypically driven size adaption (Young, 1990; Imai et al., 2015), we still note that a clear link to changing nutrient levels within the upwelling cell is becoming apparent. Imai et al. (2015) further hypothesized that the size shift is related to nutrient increases within the Indo-Pacific. Based on our records of high-nutrient conditions and likely at least intermittent seasonal eutrophication persisting from at least 11 Ma, we cannot completely follow their hypotheses that increasing nutrient levels within the surface ocean were the sole driver for this size shift. Therefore, we propose that changing nutrient limitation within the mixed layer may have played an important, as-of-yet unconsidered, role in defining the predominant assemblage structure within the WAS upwelling system during the Middle and Late Miocene (Fig. 7).

5.4   Contextualizing the primary drivers for plankton community shifts

The modern productivity patterns and oxygen depletion in the northwestern Indian Ocean differ significantly from those observed in the studied period. For example, the increase in Mn content in the Maldives in the Pliocene (Betzler et al., 2016) suggests a significant reduction in Mn redirection, which continued until today. This is indeed visible in present-day oceanographic records, where elevated Mn concentrations are only found near the margins of the Arabian Sea (ThiDieuVu and Sohrin, 2013). Meanwhile, denitrification in the Eastern Arabian Sea appears to have only become significant during the Pliocene (Tripathi et al., 2017). These changes in productivity patterns thus may indicate that the WAS was potentially more productive during the Late Miocene than today and potentially even supported an expanded OMZ (Dickens and Owen, 1999, 1994).

Despite that, we note that even in the most productive parts of the Arabian Sea conditions are rarely eutrophic (Fig. 1a). As such, ascribing permanent eutrophic or even mesotrophic conditions to any of these assemblages is unlikely to be reasonable. On the other hand, nannofossil assemblages such as TG 3 with combined diatom occurrences possibly indicate the prevalence of mesotrophic and eutrophic conditions. Diatoms are generally less adapted to low nutrient levels, requiring higher P and N levels than coccolithophores to form blooms (Hutchins and Bruland, 1998; Litchman et al., 2006). If enough nutrients (including Si) are available, they tend to outcompete coccolithophores quickly and begin to dominate

the mineralizing phytoplankton community (Schiebel et al., 2004; Brzezinski, 1985; Closset et al., 2021). Based on modern analogues, it seems likely that shifts in the nutrient content of upwelling waters may have played an important role in controlling the observed patterns in the plankton community along the WAS during the Middle to Late Miocene. In particular, after 13 Ma, a sustained and stable SAM regime seems to have existed during the Northern Hemisphere summer (Betzler et al., 2016). To disentangle these patterns, we focus on understanding observed patterns of the two dominant phytoplankton groups present within our record, with the context of their ecological preferences and primary nutrient requirements within our study interval.

The co-occurrence of diatoms, discoasterids, and sphenoliths in the upper part of the studied interval (Fig. 5) suggests that while nutrient levels were high, upwelling was likely highly seasonal. For the WAS, high seasonality may result from strengthening summer monsoon winds with no changes in winter monsoon winds (Schiebel et al., 2004; Rixen et al., 2019b; Sarr et al., 2022). Increasing summer but stable or absent winter monsoon conditions are likely the result of increased cooling in the Southern Hemisphere (Bialik et al., 2020a; Gadgil, 2018; Sarr et al., 2022). This asymmetric cooling strengthened the summer monsoon compared to the winter monsoon system, which only intensified ∼ 7 Ma (Gupta and Thomas, 2003; Holbourn et al., 2018; Rixen et al., 2019b).

The variability in wind and upwelling intensity and their interaction with nutrient availability thus likely also affected the community structure and size variability of primary producers on longer geological timescales. The community structure of primary producers then exerted control on first-level consumers, such as planktonic foraminifera.

Upwelling-derived TOC accumulation, primary productivity assemblages, and upwelling-indicative foraminifera show distinctive patterns, which are, however, not in complete agreement with wind proxies and the suggested expansion of the OMZ around 13 Ma (Betzler et al., 2016). These discrepancies resulted in a long-standing debate about the validity and usefulness of upwelling proxies as monsoonal indicators (Betzler et al., 2016; Clift and Webb, 2018; Bialik et al., 2020a; Yang et al., 2020; Sarr et al., 2022). We propose that this disagreement is primarily due to inadequate treatment of nutrient limitation and nutrient supply in conjunction with wind speed when evaluating primary productivity in the WAS (Figs. 5, 7).

Modern-day upwelling zones in the low to middle latitudes are generally well supplied in macro-nutrients, resulting in iron-limited environments or other micro- and nano-nutrient limitations (Moore et al., 2013). However, currently the fringing areas of upwelling zones are commonly N-limited through increased denitrification in underlying OMZs (Moore et al., 2013; Bristow et al., 2017; Anju et al., 2020; Buchanan et al., 2021; Ustick et al., 2021; Buttay et al., 2022). Within the WAS upwelling zone, major
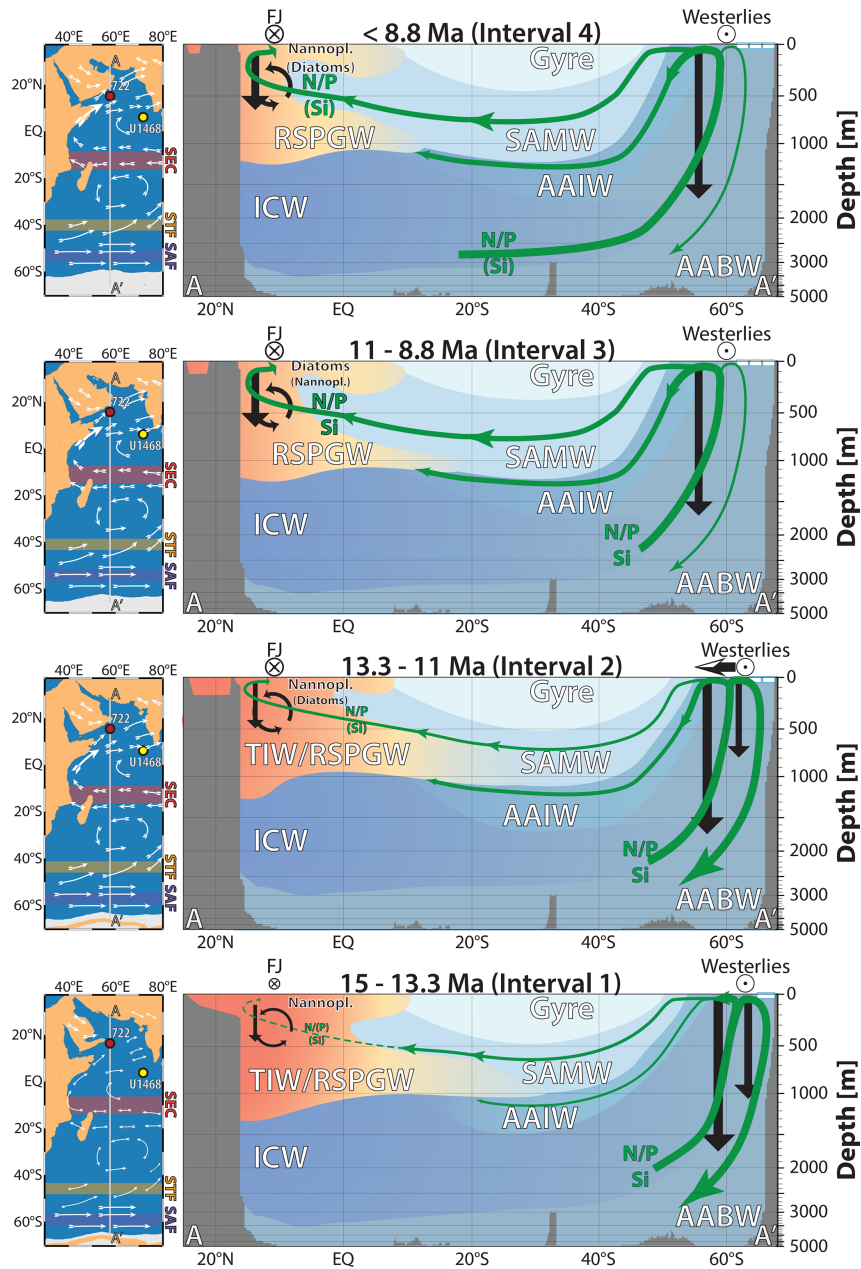
Figure 7. Envisioned progression of upwelling along the Oman margin based on the paleogeography of Cao et al. (2017), adapted with regional information (Rögl, 1999; Bialik et al., 2019; Reuter et al., 2009, 2008), combined with hypothesized changing intermediate water-based nutrient supply throughout the study interval (ca. 15–8.8 Ma). The figure also shows the hypothesized change in water masses over the study interval. Orange shading represents local water masses forming in the northern Indian Ocean and migrating southward. The retreat of local warm and high-salinity waters thus allows Antarctic Intermediate Waters to progressively migrate further in the Arabian Sea where they begin to dominate upwelling by ca. 11 Ma. The shading of the water masses represents their progressive intermixing with each other. Water masses shown are the Tethyan Intermediate Water (TIW), the Red Sea and Persian Gulf Intermediate Waters (RSPGW), Indian Central Water (ICW), southern Indian Ocean gyre waters (Gyre), sub-Antarctic Mode Water (SAMW), Antarctic Intermediate Water (AAIW), and Antarctic Bottom Water (AABW). In addition, note the corresponding hypothesized changes in nutrient (N, P, and Si) transport – visualized by green arrows – following the proposed northward migration of the Southern Hemisphere westerlies due to sea ice expansion after 12 Ma (Groeneveld et al., 2017). Hypothesized changes in nutrient transport are based on model studies, which predict reduced low-latitude productivity during warmer climates (Laufkötter and Gruber, 2018; Moore et al., 2018). Black arrows indicate the changes in the fluxes and hypothesized recycling of organic matter within the WAS upwelling zone.

nutrients N, P, and to some degree minor nutrients such as Si are replenished through local recycling and intermixing with deep and intermediate water masses originating from Antarctica (Fig. 7; Sarmiento et al., 2004; Meisel et al., 2011; Sarmiento, 2006; Laufkötter and Gruber, 2018). Iron, a key micronutrient, is primarily supplied through dust and riverine influxes from surrounding continental sources (Kunkelova et al., 2022; Moore et al., 2013; Guieu et al., 2019).

Accepting that the wind regime had reached peak intensity by 13 Ma following a gradual increase from the end of the MCO (Betzler et al., 2016, 2018), the significant increase in diatom abundance and TOC accumulation after 12 Ma is not contemporary. Therefore, the availability of nutrients and the nutrient composition also played a key role in defining the variability between coccolithophore and diatom abundances within the WAS upwelling cell. Moreover, the shift in the reticulofenestrid morphotypes (Fig. 5) may also be linked to the state of nutrient limitation. Paasche (1998) also has shown that modern-day coccolithophores tend to increase the formation of small placoliths during N-limitation.

Therefore, the shift towards higher primary productivity after 12 Ma, including the first record of diatoms at Site 722, may indicate a change in nutrient composition along the WAS without necessitating a change in monsoon wind strength. Notably, during this time, the northward expansion of the Southern Hemisphere westerlies shifted the position of the polar and sub-Antarctic frontal system (Fig. 6). In particular, the Late Miocene sea ice expansion after 11 Ma strongly affected the Antarctic frontal system and, in turn, the nutrient enrichment of intermediate waters formed in this region (Groeneveld et al., 2017; Bijl et al., 2018; Laufkötter and Gruber, 2018). Here we propose that changes in the mode of intermediate-water formation significantly increased the nutrient availability in intermediate waters in the Antarctic frontal system, resulting in modern-like downwelling dynamics around Antarctica (Fig. 7). Furthermore, many modelling studies support the assumption that climatic changes affecting the Antarctic frontal system can strongly influence global productivity patterns (Sarmiento et al., 2004; Laufkötter and Gruber, 2018; Moore et al., 2018; Taucher et al., 2022). We therefore propose that the Middle to Late Miocene productivity changes in the WAS offer compelling evidence for this hypothesis.

5.5 Synthesizing Miocene nutrient transport and monsoonal upwelling

Thus far, the discussion has focused on local aspects of the record in Site 722 in the WAS and northwestern Indian Ocean. However, the interconnected nature of the oceanic circulation and nutrient rejuvenation system means that critical mechanisms may be overlooked without a global perspective. For example, modelling evidence for nutrient transport and nutrient enrichment in low-latitude upwelling cells allows for the construction of a timeline of changes along the WAS and their interaction with plankton communities. Moreover, a complete oceanic perspective allows for contextualization into the broader evolution of the ocean-atmosphere system.

Initial plankton community structures agree with a generally low nutrient regime in a somewhat muted wind regime, based on a large amount of deep-thermocline-dwelling taxa in the foraminifera community, likely following phytoplankton primary productivity in the deeper photic zone (Lessa et al., 2020). In addition, the mixed layer is dominated by a diverse nannofossil assemblage (H'-diversity of around 1.5 within intervals 1 and 2). During the MMCT, wind shear strengthened by 13 Ma, resulting in a significant global shift in ocean–atmospheric circulation exemplified in the global reorganization of carbonate platform geometries and thermocline deepening and ventilation at Site 722, as shown by the increase in mixed-layer-dwelling planktonic foraminifera (Betzler et al., 2016, 2018; Betzler and Eberli, 2019; Lessa et al., 2020).

Modelling studies for the WAS link the initial intensification of upwelling and wind shear to a combination of increased latitudinal temperature gradients and the emergence of the Arabian Peninsula during the Middle Miocene (Zhang et al., 2014; Sarr et al., 2022; Yang et al., 2020). Notably, while OMZ expansion and Mn redirection are evident since at least ∼ 14 Ma at Site 722 (Bialik et al., 2020a), available productivity records support at most intermittently mesotrophic and likely P- and N-limited conditions before ∼ 12 Ma (Fig. 5). We thus propose that the upwelling cell in the WAS was wholly influenced by strong post-MMCT winds by 13 Ma. Productivity was still limited by the upwelling of comparably low-nutrient intermediate waters of local origin (Fig. 7). Likely originating in the marginal seas of the northwestern Indian Ocean, these water masses may have been remnants of the Tethyan Intermediate Water (TIW). While the Tethyan Seaway had terminated between 14 and 15 Ma (Bialik et al., 2019), TIW or a similar high-salinity mass (Woodruff and Savin, 1989; Smart et al., 2007) was still affecting the Northern Indian Ocean until at least 12 Ma. This remnant TIW can be considered a more potent form of the modern Red Sea and Persian Gulf Intermediate Waters (RSPGW; Fig. 7). These warm and salty intermediate waters may have played a much more substantial role in the WAS during the early stages of the uplift of the Arabian Peninsula (Woodruff and Savin, 1989; Tomczak and Godfrey, 2003; Chowdary et al., 2005; Smart et al., 2007; Acharya and Panigrahi, 2016). The influence of remnant TIW would also align with the high abundance of thermocline-dwelling taxa until 12 Ma, which we infer to be representative of a shallow and/or a poorly ventilated thermocline (Sexton and Norris, 2011; Lessa et al., 2020).

It thus seems likely that late Middle Miocene WAS upwelling may have been relatively nutrient poor. We speculate that these water masses may have suppressed primary productivity, muting the influence of the increasing Find-

later Jets and the emerging Arabian Peninsula (e.g. Sarr et al., 2022) compared to today. Invoking significant TIW upwelling until at least 12 Ma would further reconcile the discrepancy between the occurrence of drift deposits in the Maldives, and thus strong monsoon winds and the first clear evidence for strong upwelling in the WAS, with the abundance increase in upwelling indicative planktonic foraminifera (e.g. *G. bulloides*; Fig. 5) and the first occurrence of diatoms at Site 722 (Fig. 5; Kroon et al., 1991; Huang et al., 2007b; Gupta et al., 2015; Bialik et al., 2020a). This change in nutrient availability is also reflected by a contemporary increase in medium-sized reticulofenestrids (*R. antarctica* and *R. haqii*), which are generally assumed to reflect higher nutrient availability due to upwelling (Fig. 5; Auer et al., 2019, and references therein).

Productivity in the WAS thereby only began to increase as remnant TIW got progressively supplanted by other more nutrient-rich water masses. At present, the waters upwelling in the Arabian Sea are primarily regarded to be ICW, which therefore also includes IIW, SAMW, and AAIW (You, 1997, 1998; Böning and Bard, 2009; Munz et al., 2017; Chinni and Singh, 2022). Today, AAIW and SAMW, forming in the northern branch of the Antarctic Divergence, control up to 75 % of low-latitude productivity (Sarmiento et al., 2004). We hypothesize that the increasing formation of AAIW and SAMW following the northward shift of the westerlies around 12 Ma (Fig. 6) may have modulated low-latitude productivity (Groeneveld et al., 2017; Laufkötter and Gruber, 2018; Moore et al., 2018; Taucher et al., 2022). This time also aligns well with the proposed inception of the northward shift of Southern Hemisphere climate belts and the invigoration of the South Equatorial Current (LeHouedec et al., 2012; Reuter et al., 2019). Following that, it can also be assumed that by 12 Ma the northward expansion of the Southern Hemisphere westerlies resulted in a near-modern Antarctic Divergence (Groeneveld et al., 2017; Laufkötter and Gruber, 2018).

This global change in circulation patterns was fully established by 11 Ma, with cool nutrient-rich SAMW and AAIW waters reaching Site 722, evidenced by a further SST drop (Zhuang et al., 2017). This resulted in the highest productivity in the WAS upwelling cell during the Miocene (Figs. 5–7). The Late Miocene high-productivity interval in the WAS is thus the result of intense summer-monsoon-dominated SAMW and AAIW upwelling, driven by the Findlater Jets and forced by steep latitudinal temperature gradients and favourable tectonic conditions on the Arabian Peninsula (Pound et al., 2012; Zhang et al., 2014; Sarr et al., 2022). Summer months were thus characterized by eutrophic P-, N-, and potentially Si-enriched waters, allowing the proliferation of diatoms and other siliceous organisms. Winter months, in contrast, favoured the accumulation of deep-dwelling discoasterids that utilized the nutrient-rich waters below a relatively deeper winter thermocline. Higher abundances of mixed-layer dwelling taxa also reflect the increased mixed-layer depth (Fig. 5). Expanding SAMW- and

AAIW-fuelled high productivity that consequently also resulted in the highest recorded TOC fluxes between 11–10 Ma and a substantial OMZ expansion deep into the equatorial Indian Ocean (Dickens and Owen, 1994; Bialik et al., 2020a). Increasing OMZs also resulted in a global increase in denitrification, which is well-recorded in foraminifer-bound δ^{15}N records, showing a trend from more oxygenated intermediate waters during the MCO to lower oxygenated waters in the Late Miocene in the Indo-Pacific (Auderset et al., 2022).

By 10 Ma, OMZs had reached a critical threshold, leading to another substantial change in nutrient conditions within the WAS upwelling. Through increased denitrification in the OMZ underlying the upwelling cell, nitrate and ammonia were lost through bacterial conversion to N_2 (Sigman and Fripiat, 2019). Strong denitrification subsequently led to increasingly N-limited water masses upwelling within the WAS. Although concrete evidence is only presented for the WAS, these patterns could also have occurred globally, considering the clear evidence for decreasing ocean oxygenation during the Late Miocene (Auderset et al., 2022). The Late Miocene N-limitation in the WAS upwelling cell is chiefly expressed by a decline in diatom abundances after 10 Ma, in conjunction with overall community shifts in the nannofossil assemblage. Total upwelling intensity also remained consistently high, as indicated by the available SST record of Zhuang et al. (2017). Primary productivity thus remained relatively high, which is characterized by the continued presence and even dominance of large reticulofenestrids, diatoms, and the continuously high TOC concentration within the sediment (often > 1 wt %; Fig. 3). We thus assume that the drop in diatom abundance and intermittent decline in δ^{15}N values at Site 722 (Figs. 3, 5) were not caused by decreasing upwelling intensity but rather a decline in P and Si availability and thus declining export of diatom-derived organic matter. The increase in sphenoliths within our Site 722 record (Fig. 5) could indicate increased environmental stress within the nannofossil assemblage (Wade and Bown, 2006). Sphenoliths are likely not a good indicator of long-term stratification changes (Karatsolis and Henderiks, 2023) in highly seasonal upwelling regimes like the WAS, as high TOC and thus sustained but lower diatom fluxes indicate continued upwelling after 10 Ma at Site 722. Sustained seasonal upwelling and high organic matter export (Fig. 3) are further inferred by decreasing organic carbon δ^{13}C throughout this interval (Bialik et al., 2020a, and references therein).

By 8.8 Ma, the adaption of smaller reticulofenestrids may result in an evolutionary adaption to the continued N-limited nutrient availability in the WAS. We base this interpretation on the nutrient adaption of coccolithophorids based on modern culture experiments (Paasche, 1998). Although somewhat anecdotal, these offer the currently best explanation to reconcile the recorded history of Site 722 upwelling changes with the stark shifts in reticulofenestrids size ranges. It should be noted that these shifts have been recorded throughout the middle and low latitudes of the Indo-Pacific (Young,

1990; Imai et al., 2015). However, the full impact of this hypothesis needs to be tested further.

The data compilation of Young (1990) further shows that the recorded Late Miocene size shift was primarily limited to the low and middle latitudes, with larger reticulofenestrids persisting within in the higher latitudes. We propose that the transition in *Reticulofenestra* morphology from large to small morphotypes thus primarily represents a significant shift in nutrient limitation rather than total nutrient availability within the middle to low latitudes. We further argue that this turnover reflects N-limitation within the low and middle latitudes due to sustained and intense denitrification after 12 Ma (Auderset et al., 2022). Further studies, particularly on ultrastructural morphotaxonomy of reticulofenestrids, will be needed to fully disentangle the implications of the proposed N-limited nannofloral turnover.

The highly opportunistic small *Reticulofenestra* morphotype was subsequently also able to sustain phytoplankton blooms in the WAS, as evidenced by the significant increase in nannofossils within the sediment (Fig. 5). Furthermore, the high mass of small coccolith cells potentially also contributed to the re-establishment of strong denitrification, as evidenced by a rise in δ^{15}N values after 8.8 Ma (Fig. 3), as their additional biomass contributed to OMZ re-expansion. Detailed records of Late Miocene OMZ strength throughout the Indian Ocean will be necessary to fully quantify the impact on local upwelling. Local tectonics also began to modify the region configuration at this time (Rodriguez et al., 2014), leading to bottom current intensification (Rodriguez et al., 2016), which may have also modulated subsequent OMZ dynamics (Dickens and Owen, 1999).

6 Conclusions

We present fully quantitative nannofossil and planktonic foraminifera assemblage data with diatom frustule abundances for Site 722. Within a multi-proxy framework, these novel data allowed us to disentangle the complex and long-debated changes within the upwelling system of the WAS in the Middle to Late Miocene. We show that the Findlater Jets, and thus Indian Summer Monsoon wind strength, are the primary drivers of upwelling. However, wind-driven upwelling is also clearly modulated by local and global water mass changes and changing nutrient fluxes. In particular, changing nutrient transport through intermediate waters has had a significant – until now unconsidered – impact on primary productivity patterns and plankton communities over the Middle and Late Miocene in the Indian Ocean. We therefore reach the following key conclusions.

1. The expansion and evolution of upwelling within the WAS as a complex interplay of regional tectonics, global climate, and ice volume changes affected upwelling intensity and nutrient availability. The present study emphasizes that wind and nutrient changes are intrinsically related but do not necessarily operate in tandem on longer supra-Milankovitch timescales. It is, therefore, crucial to consider both water mass changes and atmospheric conditions when investigating past wind-driven upwelling regimes.

2. The interaction first invigorated monsoonal circulation after the MMCT before resulting in the reorganization of intermediate water circulation, controlled by the inception of a near-modern configuration of the Antarctic Divergence, which supplied nutrient-rich intermediate waters to the low latitudes.

3. These processes led to the progressive establishment of near-modern nutrient transport within the Indian Ocean by 12 to 11 Ma. Furthermore, these changes acted with denitrification in expanding global OMZs (Auderset et al., 2022) to increase N-limitation and subsequent adaption of coccolithophorids to the new nutrient conditions in the middle to low latitudes.

4. We provide a timeline of events that agrees with global climatic and local productivity patterns, which are all linked through the invigoration of upwelling cells and nutrient fluxes through intermediate water masses into the lower latitudes. In particular, past changes in intermediate water mass circulation, replenishment, and expansion appear to be a key – and critically understudied – aspect within paleoceanography and paleoclimatology that is crucial to understanding past and thereby future low-latitude productivity.

Author contributions. GA designed the study, acquired funding, conducted nannofossil counts and statistics, wrote the first draft, edited the text, and drafted the figures. OMB designed the study, performed statistical analyses, wrote the first draft, edited the text, and helped draft the figures. MEA performed planktonic foraminifera taxonomic analysis and assemblage interpretation and contributed to the first draft of the text. NVV helped draft the figures, contributed to data interpretation, and edited the final draft of the manuscript. WEP supervised and conducted foraminiferal analysis and contributed to writing and editing of the text.

References

Acharya, S. S. and Panigrahi, M. K.: Eastward shift and maintenance of Arabian Sea oxygen minimum zone: Understanding the paradox, Deep-Sea Res. Pt. I, 115, 240–252, https://doi.org/10.1016/j.dsr.2016.07.004, 2016.

Agnini, C., Monechi, S., and Raffi, I.: Calcareous nanno-fossil biostratigraphy: historical background and application in Cenozoic chronostratigraphy, Lethaia, 50, 447–463, https://doi.org/10.1111/let.12218, 2017.

Alam, M., Tripti, M., Gurumurthy, G. P., Sohrin, Y., Tsujisaka, M., Singh, A. D., Takano, S., and Verma, K.: Palaeoredox reconstruction in the eastern Arabian Sea since the late Miocene: Insights from trace elements and stable isotopes of molybdenum ($\delta^{98}/^{95}$Mo) and tungsten ($\delta186/184$W) at IODP Site U1457 of Laxmi Basin, Palaeogeogr. Palaeocl., 587, 110790, https://doi.org/10.1016/j.palaeo.2021.110790, 2022.

Anju, M., Sreeush, M. G., Valsala, V., Smitha, B. R., Hamza, F., Bharathi, G., and Naidu, C. V.: Understanding the Role of Nutrient Limitation on Plankton Biomass Over Arabian Sea Via 1-D Coupled Biogeochemical Model and Bio-Argo Observations, J. Geophys. Res.-Oceans, 125, e2019JC015502, https://doi.org/10.1029/2019jc015502, 2020.

Aubry, M.-P.: Handbook of Cenozoic Calcareous Nannoplankton, Book 1: Ortholithae (Discoasters), Micropaleontology Press, American Museum of Natural History, New York, 266 pp., 1984.

Aubry, M.-P.: Handbook of Cenozoic Calcareous Nannoplankton, Book 2: Ortholithae (Catinasters, Ceratoliths, Rhabdoliths), Micropaleontology Press, American Museum of Natural History, New York, 279 pp., 1988.

Aubry, M.-P.: Handbook of Cenozoic Calcareous Nannoplankton, Book 3: Ortholithae (Pentaliths, and others) Heliolithae (Fasciculiths, Sphenoliths and others), Micropaleontology Press, American Museum Natural History, New York, 279 pp., 1989.

Aubry, M.-P.: Handbook of Cenozoic Calcareous Nannoplankton, Book 4: Heliolithae (Helicoliths, Cribriliths, Lopadoliths and others), Micropaleontology Press, American Museum of Natural History, New York, 381 pp., 1990.

Aubry, M.-P.: Handbook of Cenozoic Calcareous Nannoplankton, Book 5: Heliolithae (Zygoliths and Rhabdoliths), Micropaleontology Press, American Museum of Natural History, New York, 368 pp., 1999.

Aubry, M.-P.: A major Pliocene coccolithophore turnover: Change in morphological strategy in the photic zone, vol. 424, Geological Society of America, 25–51, https://doi.org/10.1130/2007.2424(02), 2007.

Aubry, M.-P.: Coccolithophores: Cenozoic Discoasterales—Biology, Taxonomy, Stratigraphy, SEPM Society for Sedimentary Geology, 14, 460 pp., https://doi.org/10.2110/sepmcsp.14, 2021.

Auderset, A., Moretti, S., Taphorn, B., Ebner, P.-R., Kast, E., Wang, X. T., Schiebel, R., Sigman, D. M., Haug, G. H., and Martiìnez-Garciìa, A.: Enhanced ocean oxygenation during Cenozoic warm periods, Nature, 609, 77–82, https://doi.org/10.1038/s41586-022-05017-0, 2022.

Auer, G., Piller, W. E., and Harzhauser, M.: High-resolution calcareous nannoplankton palaeoecology as a proxy for small-scale environmental changes in the Early Miocene, Mar. Micropaleontol., 111, 53–65, https://doi.org/10.1016/j.marmicro.2014.06.005, 2014.

Auer, G., Piller, W. E., and Harzhauser, M.: Two distinct decadal and centennial cyclicities forced marine upwelling intensity and precipitation during the late Early Miocene in central Europe, Clim. Past, 11, 283–303, https://doi.org/10.5194/cp-11-283-2015, 2015.

Auer, G., De Vleeschouwer, D., Smith, R. A., Bogus, K., Groeneveld, J., Grunert, P., Castañeda, I. S., Petrick, B., Christensen, B., Fulthorpe, C., Gallagher, S. J., and Henderiks, J.: Timing and Pacing of Indonesian Throughflow Restriction and Its Connection to Late Pliocene Climate Shifts, Paleoceanogr. Paleocl., 34, 635–657, https://doi.org/10.1029/2018pa003512, 2019.

Auer, G., Bialik, O. M., Antoulas, M.-E., Vogt-Vincent, N., and Piller, W. E.: Quantitative nannofossil assemblage and planktonic

foraminifer data for ODP Site 117-722B, PANGAEA [data set], https://doi.org/10.1594/PANGAEA.962198, 2023.

Avinash, K., Manjunath, B. R., and Kurian, P. J.: Glacial-interglacial productivity contrasts along the eastern Arabian Sea: Dominance of convective mixing over upwelling, Geosci. Front., 6, 913–925, https://doi.org/10.1016/j.gsf.2015.03.003, 2015.

Aze, T., Ezard, T. H. G., Purvis, A., Coxall, H. K., Stewart, D. R. M., Wade, B. S., and Pearson, P. N.: A phylogeny of Cenozoic macroperforate planktonic foraminifera from fossil data, Biol. Rev., 86, 900–927, https://doi.org/10.1111/j.1469-185x.2011.00178.x, 2011.

Backman, J., Raffi, I., Rio, D., Fornaciari, E., and Pälike, H.: Biozonation and biochronology of Miocene through Pleistocene calcareous nannofossils from low and middle latitudes, Newsl. Stratigr., 45, 221–244, https://doi.org/10.1127/0078-0421/2012/0022, 2012.

Backman, J., Raffi, I., Ciummelli, M., and Baldauf, J.: Species-specific responses of late Miocene Discoaster spp. to enhanced biosilica productivity conditions in the equatorial Pacific and the Mediterranean, Geo.-Mar. Lett., 33, 285–298, https://doi.org/10.1007/s00367-013-0328-0, 2013.

Baldauf, J. G., Barron, J. A., Ehrmann, W. U., Hempel, P., and Murray, D.: Synthesis of Results from Scientific Drilling in the Indian Ocean, Geophys. Monogr. Ser., 70, 335–349, https://doi.org/10.1029/gm070p0335, 1992.

Balun, A., Field, D. B., Redondo-Rodriguez, A., and Weeks, S. J.: Greenhouse gas, upwelling-favorable winds, and the future of coastal ocean upwelling ecosystems, Glob. Change Biol., 16, 1213–1228, https://doi.org/10.1111/j.1365-2486.2009.02094.x, 2010.

Basavani, P.: Findlater Jet Climatology In Summer Monsoon: Its Role On Onset, Progress And Relation With Air Sea Interaction Parameters Over Arabian Sea, PhD thesis, Department of Physics, Acharya Nagarjuna University, 184 pp., http://hdl.handle.net/10603/49178 (last access: 16 October 2023), 2013.

Beltran, C., Rousselle, G., Backman, J., Wade, B. S., and Sicre, M.-A.: Paleoenvironmental conditions for the development of calcareous nannofossil acme during the late Miocene in the eastern equatorial Pacific, Paleoceanography, 29, 210–222, https://doi.org/10.1002/2013pa002506, 2014.

Berggren, W. A., Kennett, J. P., and Srinivasan, M. S.: Neogene Planktonic Foraminifera: A Phylogenetic Atlas, Micropaleontology, 31, 94, https://doi.org/10.2307/1485586, 1985.

Betzler, C. and Eberli, G. P.: Miocene start of modern carbonate platforms, Geology, 47, 771–775, https://doi.org/10.1130/g45994.1, 2019.

Betzler, C., Eberli, G. P., Kroon, D., Wright, J. D., Swart, P. K., Nath, B. N., Alvarez-Zarikian, C. A., Alonso-García, M., Bialik, O. M., Blättler, C. L., Guo, J. A., Haffen, S., Horozal, S., Inoue, M., Jovane, L., Lanci, L., Laya, J. C., Mee, A. L. H., Lüdmann, T., Nakakuni, M., Niino, K., Petruny, L. M., Pratiwi, S. D., Reijmer, J. J. G., Reolid, J., Slagle, A. L., Sloss, C. R., Su, X., Yao, Z., and Young, J. R.: The abrupt onset of the modern South Asian Monsoon winds., Sci. Rep., 6, 29838, https://doi.org/10.1038/srep29838, 2016.

Betzler, C., Eberli, G. P., Lüdmann, T., Reolid, J., Kroon, D., Reijmer, J. J. G., Swart, P. K., Wright, J., Young, J. R., Alvarez-Zarikian, C., Alonso-García, M., Bialik, O. M., Blättler, C. L., Guo, J. A., Haffen, S., Horozal, S., Inoue, M., Jovane, L.,

Lanci, L., Laya, J. C., Mee, A. L. H., Nakakuni, M., Nath, B. N., Niino, K., Petruny, L. M., Pratiwi, S. D., Slagle, A. L., Sloss, C. R., Su, X., and Yao, Z.: Refinement of Miocene sea level and monsoon events from the sedimentary archive of the Maldives (Indian Ocean), Prog. Earth Planet. Sci., 5, 5, https://doi.org/10.1186/s40645-018-0165-x, 2018.

Bialik, O. M., Frank, M., Betzler, C., Zammit, R., and Waldmann, N. D.: Two-step closure of the Miocene Indian Ocean Gateway to the Mediterranean, Sci. Rep., 9, 8842–8852, https://doi.org/10.1038/s41598-019-45308-7, 2019.

Bialik, O. M., Auer, G., Ogawa, N. O., Kroon, D., Waldmann, N. D., and Ohkouchi, N.: Monsoons, Upwelling, and the Deoxygenation of the Northwestern Indian Ocean in Response to Middle to Late Miocene Global Climatic Shifts, Paleoceanogr. Paleocl., 35, e2019PA003762, https://doi.org/10.1029/2019pa003762, 2020a.

Bialik, O. M., Reolid, J., Betzler, C., Eberli, G. P., and Waldmann, N. D.: Source shifts to periplatform deposits during the early to middle Miocene in response to climatic and oceanographic forcing, Maldives, western Indian Ocean, Palaeogeogr. Palaeocl., 559, 109969, https://doi.org/10.1016/j.palaeo.2020.109969, 2020b.

Bialik, O. M., Jarochowska, E., and Grossowicz, M.: Ordination analysis in sedimentology, geochemistry and palaeoenvironment–Background, current trends and recommendations, Depositional Rec., 7, 541–563, https://doi.org/10.1002/dep2.161, 2021.

Bijl, P. K., Houben, A. J. P., Hartman, J. D., Pross, J., Salabarnada, A., Escutia, C., and Sangiorgi, F.: Paleoceanography and ice sheet variability offshore Wilkes Land, Antarctica – Part 2: Insights from Oligocene–Miocene dinoflagellate cyst assemblages, Clim. Past, 14, 1015–1033, https://doi.org/10.5194/cp-14-1015-2018, 2018.

Blain, S., Leynaert, A., Tréguer, P., Chretiennot-Dinet, M.-J., and Rodier, M.: Biomass, growth rates and limitation of Equatorial Pacific diatoms, Deep-Sea Res Pt. I, 44, 1255–1275, https://doi.org/10.1016/s0967-0637(97)00014-9, 1997.

Blanc-Valleron, M. M., Pierre, C., Caulet, J. P., Caruso, A., Rouchy, J. M., Cespuglio, G., Sprovieri, R., Pestrea, S., and Stefano, E. D.: Sedimentary, stable isotope and micropaleontological records of paleoceanographic change in the Messinian Tripoli Formation (Sicily, Italy), Palaeogeogr. Palaeocl., 185, 255–286, https://doi.org/10.1016/s0031-0182(02)00302-4, 2002.

Boersma, A. and Mikkelsen, N.: Miocene-Age Primary Productivity Episodes and Oxygen Minima in the Central Equatorial Indian Ocean, in: Proceedings of the Ocean Drilling Program, Scientific Results, Vol. 115, edited by: Duncan, R. A., Backman, J., and Peterson, L. C., https://doi.org/10.2973/odp.proc.sr.115.162.1991, 1990.

Bollmann, J.: Morphology and biogeography of Gephyrocapsa coccoliths in Holocene sediments, Mar. Micropaleontol., 29, 319–350, https://doi.org/10.1016/s0377-8398(96)00028-x, 1997.

Böning, P. and Bard, E.: Millennial/centennial-scale thermocline ventilation changes in the Indian Ocean as reflected by aragonite preservation and geochemical variations in Arabian Sea sediments, Geochim. Cosmochim. Ac., 73, 6771–6788, https://doi.org/10.1016/j.gca.2009.08.028, 2009.

Bordiga, M., Bartol, M., and Henderiks, J.: Absolute nannofossil abundance estimates: Quantifying the pros and cons of

different techniques, Rev. de Micropaleontol., 58, 155–165, https://doi.org/10.1016/j.revmic.2015.05.002, 2015.

Brembu, T., Mühlroth, A., Alipanah, L., and Bones, A. M.: The effects of phosphorus limitation on carbon metabolism in diatoms, Philos. T. R. Soc. B, 372, 20160406, https://doi.org/10.1098/rstb.2016.0406, 2017.

Bristow, L. A., Mohr, W., Ahmerkamp, S., and Kuypers, M. M. M.: Nutrients that limit growth in the ocean, Curr. Biol., 27, R474–R478, https://doi.org/10.1016/j.cub.2017.03.030, 2017.

Brummer, G.-J. A. and Kučera, M.: Taxonomic review of living planktonic foraminifera, J. Micropalaeontol., 41, 29–74, https://doi.org/10.5194/jm-41-29-2022, 2022.

Brzezinski, M. A.: The Si : C : N ratio of marine diatoms: interspecific variability and the effect of some environmental variables 1, J. Phycol., 21, 347–357, https://doi.org/10.1111/j.0022-3646.1985.00347.x, 1985.

Buchanan, P. J., Aumont, O., Bopp, L., Mahaffey, C., and Tagliabue, A.: Impact of intensifying nitrogen limitation on ocean net primary production is fingerprinted by nitrogen isotopes, Nat. Commun., 12, 6214, https://doi.org/10.1038/s41467-021-26552-w, 2021.

Buttay, L., Vasseur, D. A., González-Quirós, R., and Nogueira, E.: Nutrient limitation can explain a rapid transition to synchrony in an upwelling-driven diatom community, Limnol. Oceanogr., 67, S298–S311, https://doi.org/10.1002/lno.12033, 2022.

Cao, W., Zahirovic, S., Flament, N., Williams, S., Golonka, J., and Müller, R. D.: Improving global paleogeography since the late Paleozoic using paleobiology, Biogeosciences, 14, 5425–5439, https://doi.org/10.5194/bg-14-5425-2017, 2017.

Carlson, R. E.: A trophic state index for lakes, Limnol. Oceanogr., 22, 361–369, https://doi.org/10.4319/lo.1977.22.2.0361, 1977.

Castradori, D.: Calcareous nannofossils in the basal Zanclean of the Eastern Mediterranean Sea: remarks on paleoceanography and sapropel formation, in: Proceedings of the Ocean Drilling Program, 160 Scientific Results, vol. 160, https://doi.org/10.2973/odp.proc.sr.160.005.1998, 1998.

Chaisson, W. P. and Ravelo, A. C.: Changes in upper water-column structure at Site 925, late Miocene–Pleistocene: planktonic foraminifer assemblage and isotopic evidence, in: Proceedings of the Ocean Drilling Program, 154 Scientific Results, https://doi.org/10.2973/odp.proc.sr.154.105.1997, 1997.

Chinni, V. and Singh, S. K.: Dissolved iron cycling in the Arabian Sea and sub-tropical gyre region of the Indian Ocean, Geochim. Cosmochim. Ac., 317, 325–348, https://doi.org/10.1016/j.gca.2021.10.026, 2022.

Chowdary, J. S., Gnanaseelan, C., Thompson, B., and Salvekar, P. S.: Water mass properties and transports in the Arabian Sea from Argo observations, J. Atmos. Sci., 10, 235–260, https://doi.org/10.1080/17417530600752825, 2005.

Clarke, K. R.: Non-parametric multivariate analyses of changes in community structure, Aust. J. Ecol., 18, 117–143, https://doi.org/10.1111/j.1442-9993.1993.tb00438.x, 1993.

Clift, P. D. and Webb, A. A. G.: A history of the Asian monsoon and its interactions with solid Earth tectonics in Cenozoic South Asia, Geological Society, London, Special Publications, 483, SP483.1, https://doi.org/10.1144/sp483.1, 2018.

Closset, I., McNair, H. M., Brzezinski, M. A., Krause, J. W., Thamatrakoln, K., and Jones, J. L.: Diatom response to alterations in upwelling and nutrient dynamics associated with climate forcing

in the California Current System, Limnol. Oceanogr., 66, 1578–1593, https://doi.org/10.1002/lno.11705, 2021.

Cullen, J. J.: Hypotheses to explain high-nutrient conditions in the open sea, Limnol. Oceanogr., 36, 1578–1599, https://doi.org/10.4319/lo.1991.36.8.1578, 1991.

Currie, R. I., Fisher, A. E., and Hargreaves, P. M.: Arabian Sea Upwelling, in: The Biology of the Indian Ocean, vol. 3, edited by: Zeitzschel, B. and Gerlach, S. A., 37–52, https://doi.org/10.1007/978-3-642-65468-8_4, 1973.

Dickens, G. R. and Owen, R. M.: Late Miocene-Early Pliocene manganese redirection in the central Indian Ocean: Expansion of the Intermediate Water oxygen minimum zone, Paleoceanography, 9, 169–181, https://doi.org/10.1029/93pa02699, 1994.

Dickens, G. R. and Owen, R. M.: The Latest Miocene–Early Pliocene biogenic bloom: a revised Indian Ocean perspective, Mar. Geol., 161, 75–91, https://doi.org/10.1016/s0025-3227(99)00057-2, 1999.

Dugdale, R. C.: Chemical oceanography and primary productivity in upwelling regions, Geoforum, 3, 47–61, https://doi.org/10.1016/0016-7185(72)90085-1, 1972.

E.U. Copernicus Marine Service Information (CMEMS): Global Ocean Colour (Copernicus-GlobColour), Bio-Geo-Chemical, L4 (monthly and interpolated) from Satellite Observations (1997–ongoing), Marine Data Store (MDS) [data set], https://doi.org/10.48670/moi-00281, 2023.

Falkowski, P. G.: Evolution of the nitrogen cycle and its influence on the biological sequestration of CO_2 in the ocean, Nature, 387, 272–275, https://doi.org/10.1038/387272a0, 1997.

Findlater, J.: A major low-level air current near the Indian Ocean during the northern summer, Q. J. R. Meteor. Soc., 95, 362–380, 1969.

Flower, B. P. and Kennett, J. P.: The middle Miocene climatic transition: East Antarctic ice sheet development, deep ocean circulation and global carbon cycling, Palaeogeogr. Palaeocl., 108, 537–555, https://doi.org/10.1016/0031-0182(94)90251-8, 1994.

Frigola, A., Prange, M., and Schulz, M.: Boundary conditions for the Middle Miocene Climate Transition (MMCT v1.0), Geosci. Model Dev., 11, 1607–1626, https://doi.org/10.5194/gmd-11-1607-2018, 2018.

Gadgil, S.: The monsoon system: Land–sea breeze or the ITCZ?, J. Earth Syst. Sci., 127, 1–29, https://doi.org/10.1007/s12040-017-0916-x, 2018.

Garcia, H. E., Weathers, K. W., Paver, C. R., Smolyar, I., Boyer, T. P., Locarnini, R. A., Zweng, M. M., Mishonov, A. V., Baranova, O. K., Seidov, D., and Reagan, J. R.: World Ocean Atlas 2018 Volume 3: Dissolved Oxygen, Apparent Oxygen Utilization, and Oxygen Saturation, NOAA Atlas NESDIS 83, 38 pp., 2019.

Garnesson, P., Mangin, A., Fanton d'Andon, O., Demaria, J., and Bretagnon, M.: The CMEMS GlobColour chlorophyll a product based on satellite observation: multi-sensor merging and flagging strategies, Ocean Sci., 15, 819–830, https://doi.org/10.5194/os-15-819-2019, 2019.

Gaye, B., Böll, A., Segschneider, J., Burdanowitz, N., Emeis, K.-C., Ramaswamy, V., Lahajnar, N., Lückge, A., and Rixen, T.: Glacial–interglacial changes and Holocene variations in Arabian Sea denitrification, Biogeosciences, 15, 507–527, https://doi.org/10.5194/bg-15-507-2018, 2018.

Gibbs, S., Shackleton, N., and Young, J.: Orbitally forced climate signals in mid-Pliocene nannofos-

sil assemblages, Mar. Micropaleontol., 51, 39–56, https://doi.org/10.1016/j.marmicro.2003.09.002, 2004.

Gibbs, S. J., Shackleton, N. J., and Young, J. R.: Identification of dissolution patterns in nannofossil assemblages: A high-resolution comparison of synchronous records from Ceara Rise, ODP Leg 154, Paleoceanography, 19, 1–12, https://doi.org/10.1029/2003pa000958, 2004.

Gibbs, S. J., Young, J. R., Bralower, T. J., and Shackleton, N. J.: Nannofossil evolutionary events in the mid-Pliocene: an assessment of the degree of synchrony in the extinctions of Reticulofenestra pseudoumbilicus and Sphenolithus abies, Palaeogeogr. Palaeocl., 217, 155–172, https://doi.org/10.1016/j.palaeo.2004.11.005, 2005.

Gohin, F.: Annual cycles of chlorophyll-a, non-algal suspended particulate matter, and turbidity observed from space and in-situ in coastal waters, Ocean Sci., 7, 705–732, https://doi.org/10.5194/os-7-705-2011, 2011.

Gourlan, A. T., Meynadier, L., and Allègre, C. J.: Tectonically driven changes in the Indian Ocean circulation over the last 25 Ma: Neodymium isotope evidence, Earth Planet. Sc. Lett., 267, 353–364, https://doi.org/10.1016/j.epsl.2007.11.054, 2008.

Groeneveld, J., Henderiks, J., Renema, W., McHugh, C. M., DeVleeschouwer, D., Christensen, B. A., Fulthorpe, C. S., Reuning, L., Gallagher, S. J., Bogus, K., Auer, G., Ishiwa, T., and Scientists, E. 356: Australian shelf sediments reveal shifts in Miocene Southern Hemisphere westerlies, Sci. Adv., 3, 1–8, https://doi.org/10.1126/sciadv.1602567, 2017.

Guieu, C., Azhar, M. A., Aumont, O., Mahowald, N., Levy, M., Ethé, C., and Lachkar, Z.: Major Impact of Dust Deposition on the Productivity of the Arabian Sea, Geophys. Res. Lett., 46, 6736–6744, https://doi.org/10.1029/2019gl082770, 2019.

Gupta, A. K. and Thomas, E.: Initiation of Northern Hemisphere glaciation and strengthening of the northeast Indian monsoon: Ocean Drilling Program Site 758, eastern equatorial Indian Ocean, Geology, 31, 47–50, https://doi.org/10.1130/0091-7613(2003)031<0047:IONHGA>2.0.CO;2, 2003.

Gupta, A. K., Singh, R. K., Joseph, S., and Thomas, E.: Indian Ocean high-productivity event (10–8 Ma): Linked to global cooling or to the initiation of the Indian monsoons?, Geology, 32, 753–756, https://doi.org/10.1130/g20662.1, 2004.

Gupta, A. K., Yuvaraja, A., Prakasam, M., Clemens, S. C., and Velu, A.: Evolution of the South Asian monsoon wind system since the late Middle Miocene, Palaeogeogr. Palaeocl., 438, 160–167, https://doi.org/10.1016/j.palaeo.2015.08.006, 2015.

Hall, R.: Sundaland and Wallacea: Geology, plate tectonics and palaeogeography, edited by: Gower, D., Johnson, Kenneth, Richardson, James, Rosen, Brian, Ruber, Lukas, and Williams, S., Cambridge University Press, 32–78, https://doi.org/10.1017/cbo9780511735882.005, 2012.

Hammer, Ø. and Harper, D. A. T.: Paleontological Data Analysis, 1st ed., Blackwell Publishing Ltd, ISBN 9781405115445, 2006.

Hammer, Ø., Harper, D. A. T., and Ryan, P. D.: PAST: paleontological statistics software package for education and data analysis, Palaeontol. Electron., 4, 1–9, 2001.

Haq, B. U.: Biogeographic history of Miocene calcareous nannoplankton and paleoceanography of the Atlantic Ocean, Micropaleontology, 26, 414–443, 1980.

Haq, B. U. and Lohmann, G. P.: Early Cenozoic calcareous nannoplankton biogeography of the Atlantic Ocean, Mar. Micropaleon-

tol., 1, 119–194, https://doi.org/10.1016/0377-8398(76)90008-6, 1976.

Harzhauser, M., Kroh, A., Mandic, O., Piller, W. E., Göhlich, U., Reuter, M., and Berning, B.: Biogeographic responses to geodynamics: A key study all around the Oligo–Miocene Tethyan Seaway, Special Issue: Phylogenetic Symposium 48th Phylogenetic Symposium on Historical Biogeography, 246, 241–256, https://doi.org/10.1016/j.jcz.2007.05.001, 2007.

Head, E. J. H., Harrison, W. G., Irwin, B. I., Horne, E. P. W., and Li, W. K. W.: Plankton dynamics and carbon flux in an area of upwelling off the coast of Morocco, Deep-Sea Res. Pt. I, 43, 1713–1738, https://doi.org/10.1016/s0967-0637(96)00080-5, 1996.

Holbourn, A., Kuhnt, W., Lyle, M., Schneider, L., Romero, O., and Andersen, N.: Middle Miocene climate cooling linked to intensification of eastern equatorial Pacific upwelling, Geology, 42, 19–22, https://doi.org/10.1130/g34890.1, 2014.

Holbourn, A., Kuhnt, W., Kochhann, K. G. D., Andersen, N., and Meier, K. J. S.: Global perturbation of the carbon cycle at the onset of the Miocene Climatic Optimum, Geology, 43, 123–126, https://doi.org/10.1130/g36317.1, 2015.

Holbourn, A. E., Kuhnt, W., Clemens, S. C., Kochhann, K. G. D., Jöhnck, J., Lübbers, J., and Andersen, N.: Late Miocene climate cooling and intensification of southeast Asian winter monsoon, Nat. Commun., 9, 365, https://doi.org/10.1038/s41467-018-03950-1, 2018.

Honjo, S., Dymond, J., Prell, W., and Ittekkot, V.: Monsoon-controlled export fluxes to the interior of the Arabian Sea, Deep-Sea Res. Pt. II, 46, 1859–1902, https://doi.org/10.1016/s0967-0645(99)00047-8, 1999.

House, M. A., Rea, D. K., and Janecek, T. R.: Proceedings of the Ocean Drilling Program, 121 Scientific Results, vol. 121, edited by: Weissel, J., Peirce, J., Taylor, E., and Alt, J., 211–218, https://doi.org/10.2973/odp.proc.sr.121.133.1991, 1991.

Hu, C., Lee, Z., and Franz, B.: Chlorophyll aalgorithms for oligotrophic oceans: A novel approach based on three-band reflectance difference, J. Geophys. Res.-Oceans, 117, C01011, https://doi.org/10.1029/2011jc007395, 2012.

Huang, Y., Clemens, S. C., Liu, W., Wang, Y., and Prell, W. L.: Large-scale hydrological change drove the late Miocene C4 plant expansion in the Himalayan foreland and Arabian Peninsula, Geology, 35, 531–534, 2007a.

Huang, Y., Clemens, S. C., Liu, W., Wang, Y., and Prell, W. L.: Large-scale hydrological change drove the late Miocene C_4 plant expansion in the Himalayan foreland and Arabian Peninsula, Geology, 35, 531–534, https://doi.org/10.1130/g23666a.1, 2007b.

Hutchins, D. A. and Bruland, K. W.: Iron-limited diatom growth and Si:N uptake ratios in a coastal upwelling regime, Nature, 393, 561–564, https://doi.org/10.1038/31203, 1998.

Imai, R., Farida, M., Sato, T., and Iryu, Y.: Evidence for eutrophication in the northwestern Pacific and eastern Indian oceans during the Miocene to Pleistocene based on the nannofossil accumulation rate, Discoaster abundance, and coccolith size distribution of Reticulofenestra, Mar. Micropaleontol., 116, 15–27, https://doi.org/10.1016/j.marmicro.2015.01.001, 2015.

Imai, R., Sato, T., and Iryu, Y.: Calcareous nannofossil assemblages of the upper Miocene to Pliocene Shimajiri Group on Okinawajima, Ryukyu Islands, southwestern Japan, J. Asian Earth Sci., 135, 16–24, https://doi.org/10.1016/j.jseaes.2016.12.011, 2017.

Itou, M., Ono, T., Oba, T., and Noriki, S.: Isotopic composition and morphology of living Globorotalia scitula: a new proxy of sub-intermediate ocean carbonate chemistry?, Mar. Micropaleontol., 42, 189–210, https://doi.org/10.1016/s0377-8398(01)00015-9, 2001.

Jatiningrum, R. S. and Sato, T.: Sea-Surface Dynamics Changes in the Subpolar North Atlantic Ocean (IODP Site U1314) during Late Pliocene Climate Transition Based on Calcareous Nannofossil Observation, Open J. Geol., 7, 1538–1551, https://doi.org/10.4236/ojg.2017.710103, 2017.

Karatsolis, B.-T. and Henderiks, J.: Late Neogene nannofossil assemblages as tracers of ocean circulation and paleoproductivity over the NW Australian shelf, Clim. Past, 19, 765–786, https://doi.org/10.5194/cp-19-765-2023, 2023.

Keller, G. and Barron, J. A.: Paleoceanographic implications of Miocene deep-sea hiatuses, Gsa Bulletin, 94, 590–613, https://doi.org/10.1130/0016-7606(1983)94<590:PIOMDH>2.0.CO;2, 1983.

Kennett, J. P. and Srinivasan, M. S.: Neogene Planktonic Foraminifera: A Phylogenetic Atlas, Hutchinson Ross, Distributed by worldwide by Van Nostrand Reinhold, Stroudsburg, PA, 265 pp., ISBN 9780879330705, 1983.

Krapivin, V. F. and Varotsos, C. A.: Modelling the CO_2 atmosphere-ocean flux in the upwelling zones using radiative transfer tools, J. Atmos. Sol.-Terr. Phy., 150, 47–54, https://doi.org/10.1016/j.jastp.2016.10.015, 2016.

Kroon, D., Steens, T. N. F., and Troelstra, S. R.: Proceedings of the Ocean Drilling Program, 117 Scientific Results, Proc. Ocean Drill. Program., 117, 257–263, https://doi.org/10.2973/odp.proc.sr.117.126.1991, 1991.

Kuhnt, W., Holbourn, A., Xu, J., Opdyke, B., Deckker, P. D., Röhl, U., and Mudelsee, M.: Southern Hemisphere control on Australian monsoon variability during the late deglaciation and Holocene, Nat. Commun., 6, 5916, https://doi.org/10.1038/ncomms6916, 2015.

Kunkelova, T., Crocker, A. J., Jewell, A. M., Breeze, P. S., Drake, N. A., Cooper, M. J., Milton, J. A., Hennen, M., Shahgedanova, M., Petraglia, M., and Wilson, P. A.: Dust sources in Westernmost Asia have a different geochemical fingerprint to those in the Sahara, Quaternary Sci. Rev., 294, 107717, https://doi.org/10.1016/j.quascirev.2022.107717, 2022.

Lahiri, S. P. and Vissa, N. K.: Assessment of Indian Ocean upwelling changes and its relationship with the Indian monsoon, Global Planet. Change, 208, 103729, https://doi.org/10.1016/j.gloplacha.2021.103729, 2022.

Laufkötter, C. and Gruber, N.: Will marine productivity wane?, Science, 359, 1103–1104, https://doi.org/10.1126/science.aat0795, 2018.

Lee, C., Murray, D. W., Barber, R. T., Buesseler, K. O., Dymond, J., Hedges, J. I., Honjo, S., Manganini, S. J., Marra, J., Moser, C., Peterson, M. L., Prell, W. L., and Wakeham, S. G.: Particulate organic carbon fluxes: compilation of results from the 1995 US JGOFS Arabian Sea Process Study, Deep-Sea Res. Pt. II, 45, 2489–2501, https://doi.org/10.1016/s0967-0645(98)00079-4, 1998.

LeHouedec, S., Meynadier, L., and Allègre, C. J.: Nd isotope systematics on ODP Sites 756 and 762 sediments reveal major volcanic, oceanic and climatic changes in South Indian Ocean over the last 35 Ma, Earth Planet. Sc. Lett., 327–328, 29–38, https://doi.org/10.1016/j.epsl.2012.01.019, 2012.

Lessa, D., Morard, R., Jonkers, L., Venancio, I. M., Reuter, R., Baumeister, A., Albuquerque, A. L., and Kucera, M.: Distribution of planktonic foraminifera in the subtropical South Atlantic: depth hierarchy of controlling factors, Biogeosciences, 17, 4313–4342, https://doi.org/10.5194/bg-17-4313-2020, 2020.

Ling, A., Eberli, G. P., Swart, P. K., Reolid, J., Stainbank, S., Rüggeberg, A., and Betzler, C.: Middle Miocene platform drowning in the Maldives associated with monsoon-related intensification of currents, Palaeogeogr. Palaeocl., 567, 110275, https://doi.org/10.1016/j.palaeo.2021.110275, 2021.

Litchman, E., Klausmeier, C. A., Miller, J. R., Schofield, O. M., and Falkowski, P. G.: Multi-nutrient, multi-group model of present and future oceanic phytoplankton communities, Biogeosciences, 3, 585–606, https://doi.org/10.5194/bg-3-585-2006, 2006.

Lohmann, G. P. and Carlson, J. J.: Oceanographic significance of Pacific late miocene calcareous nannoplankton, Mar. Micropaleontol., 6, 553–579, https://doi.org/10.1016/0377-8398(81)90021-9, 1981.

Lübbers, J., Kuhnt, W., Holbourn, A. E., Bolton, C. T., Gray, E., Usui, Y., Kochhann, K. G. D., Beil, S., and Andersen, N.: The middle to late Miocene "Carbonate Crash" in the equatorial Indian Ocean, Paleoceanogr. Paleocl., 34, 2018PA003482, https://doi.org/10.1029/2018pa003482, 2019.

Madhupratap, M., Kumar, S. P., Bhattathiri, P. M. A., Kumar, M. D., Raghukumar, S., Nair, K. K. C., and Ramaiah, N.: Mechanism of the biological response to winter cooling in the northeastern Arabian Sea, Nature, 384, 549–552, https://doi.org/10.1038/384549a0, 1996.

Majewski, W.: Water-depth distribution of Miocene planktonic foraminifera from ODP Site 744, southern Indian Ocean, J. Foramin. Res, 33, 144–154, https://doi.org/10.2113/0330144, 2003.

McCreary, J. P., Yu, Z., Hood, R. R., Vinaychandran, P. N., Furue, R., Ishida, A., and Richards, K. J.: Dynamics of the Indian-Ocean oxygen minimum zones, Prog. Oceanogr., 112–113, 15–37, https://doi.org/10.1016/j.pocean.2013.03.002, 2013.

Meisel, S., Struck, U., and Emeis, K.-C.: Nutrient dynamics and oceanographic features in the central Namibian upwelling region as reflected in $\delta^{15}N$-signals of suspended matter and surface sediments, Foss. Rec., 14, 153–169, https://doi.org/10.1002/mmng.201100005, 2011.

Mikaelyan, A. S., Pautova, L. A., Chasovnikov, V. K., Mosharov, S. A., and Silkin, V. A.: Alternation of diatoms and coccolithophores in the north-eastern Black Sea: a response to nutrient changes, Hydrobiologia, 755, 89–105, https://doi.org/10.1007/s10750-015-2219-z, 2015.

Miller, K. G., Browning, J. V., Schmelz, W. J., Kopp, R. E., Mountain, G. S., and Wright, J. D.: Cenozoic sea-level and cryospheric evolution from deep-sea geochemical and continental margin records, Sci. Adv., 6, eaaz1346, https://doi.org/10.1126/sciadv.aaz1346, 2020.

Millero, F. J.: The Marine Inorganic Carbon Cycle, Chem. Rev., 107, 308–341, https://doi.org/10.1021/cr0503557, 2007.

Moore, C. M., Mills, M. M., Arrigo, K. R., Berman-Frank, I., Bopp, L., Boyd, P. W., Galbraith, E. D., Geider, R. J., Guieu, C., Jaccard, S. L., Jickells, T. D., Roche, J. L., Lenton, T. M., Mahowald, N. M., Marañón, E., Marinov, I., Moore, J. K., Nakatsuka, T., Os-

chlies, A., Saito, M. A., Thingstad, T. F., Tsuda, A., and Ulloa, O.: Processes and patterns of oceanic nutrient limitation, Nat. Geosci., 6, 701–710, https://doi.org/10.1038/ngeo1765, 2013.

Moore, J. K., Fu, W., Primeau, F., Britten, G. L., Lindsay, K., Long, M., Doney, S. C., Mahowald, N., Hoffman, F., and Randerson, J. T.: Sustained climate warming drives declining marine biological productivity, Science, 359, 1139–1143, https://doi.org/10.1126/science.aao6379, 2018.

Morrison, J. M., Codispoti, L. A., Gaurin, S., Jones, B., Manghnani, V., and Zheng, Z.: Seasonal variation of hydrographic and nutrient fields during the US JGOFS Arabian Sea Process Study, Deep-Sea Res. Pt. II, 45, 2053–2101, https://doi.org/10.1016/s0967-0645(98)00063-0, 1998.

Munz, P. M., Siccha, M., Lückge, A., Böll, A., Kucera, M., and Schulz, H.: Decadal-resolution record of winter monsoon intensity over the last two millennia from planktic foraminiferal assemblages in the northeastern Arabian Sea, Holocene, 25, 1756–1771, https://doi.org/10.1177/0959683615591357, 2015.

Munz, P. M., Steinke, S., Böll, A., Lückge, A., Groeneveld, J., Kucera, M., and Schulz, H.: Decadal resolution record of Oman upwelling indicates solar forcing of the Indian summer monsoon (9–6 ka), Clim. Past, 13, 491–509, https://doi.org/10.5194/cp-13-491-2017, 2017.

Naik, D. K., Saraswat, R., Lea, D. W., Kurtarkar, S. R., and Mackensen, A.: Last glacial-interglacial productivity and associated changes in the eastern Arabian Sea, Palaeogeogr. Palaeocl., 483, 147–156, https://doi.org/10.1016/j.palaeo.2016.07.014, 2017.

Nannotax 3: http://www.mikrotax.org/Nannotax3/, last access: 24 July 2023.

Negri, A. and Villa, G.: Calcareous nannofossil biostratigraphy, biochronology and paleoecology at the Tortonian/Messinian boundary of the Faneromeni section (Crete), Palaeogeogr. Palaeocl., 156, 195–209, 2000.

Nigrini, C.: Composition and Biostratigraphy of Radiolarian Assemblages from an Area of Upwelling (Northwestern Arabian Sea, Leg 117), in: Proceedings of the Ocean Drilling Program, 117 Scientific Results, vol. 117, edited by: Prell, W. J. and Niitsuma, N., 89–126, https://doi.org/10.2973/odp.proc.sr.117.132.1991, 1991.

Nikolaev, S. D., Oskina, N. S., Blyum, N. S., and Bubenshchikova, N. V.: Neogene–Quaternary variations of the "Pole–Equator" temperature gradient of the surface oceanic waters in the North Atlantic and North Pacific, Global Planet. Change, 18, 85–111, https://doi.org/10.1016/s0921-8181(98)00009-5, 1998.

Paasche, E.: Roles of nitrogen and phosphorus in coccolith formation in *Emiliania huxleyi* (Prymnesiophyceae), Eur. J. Phycol., 33, 33–42, https://doi.org/10.1080/09670269810001736513, 1998.

Paerl, H. W.: Why does N-limitation persist in the world's marine waters?, Mar. Chem., 206, 1–6, https://doi.org/10.1016/j.marchem.2018.09.001, 2018.

Pearson, P. N. and Shackleton, N. J.: Neogene multispecies planktonic foraminifer stable isotope record, Site 871, Limalok Guyot, in: Proceedings of the Ocean Drilling Program, 144 Scientific Results, edited by: Haggerty, J. A., Premoli-Silva, I., Rack, F., and McNutt, M. K., https://doi.org/10.2973/odp.proc.sr.144.054.1995, 1995.

Pearson, P. N. and Wade, B. S.: Taxonomy and stable isotope paleoecology of well-preserved planktonic foraminifera from the uppermost oligocene of Trinidad, J. Foramin. Res., 39, 191–217, https://doi.org/10.2113/gsjfr.39.3.191, 2009.

Perch-Nielsen, K.: Cenozoic Calcareous Nanofossils, in: Plankton Stratigraphy, vol. 1, edited by: Bolli, H. M., Saunders, J. B., and Perch-Nielsen, K., Cambridge University Press, 427–554, ISBN 0521367190, 1985.

Pound, M. J., Haywood, A. M., Salzmann, U., and Riding, J. B.: Global vegetation dynamics and latitudinal temperature gradients during the Mid to Late Miocene (15.97–5.33 Ma), Earth-Sci. Rev., 112, 1–22, https://doi.org/10.1016/j.earscirev.2012.02.005, 2012.

Pourmand, A., Marcantonio, F., Bianchi, T. S., Canuel, E. A., and Waterson, E. J.: A 28-ka history of sea surface temperature, primary productivity and planktonic community variability in the western Arabian Sea, Paleoceanography, 22, PA4208, https://doi.org/10.1029/2007pa001502, 2007.

Prell, W. L., Murray, D. W., Clemens, S. C., and Anderson, D. M.: Evolution and Variability of the Indian Ocean Summer Monsoon: Evidence from the Western Arabian Sea Drilling Program, edited by: Duncan, R. A., Rea, D. K., Kidd, R. B., von Rad, U., and Weissel, J. K., 447–469, https://doi.org/10.1029/gm070p0447, 1992.

Raven, J. A. and Falkowski, P. G.: Oceanic sinks for atmospheric CO_2, Plant Cell Environ., 22, 741–755, https://doi.org/10.1046/j.1365-3040.1999.00419.x, 1999.

Regenberg, M., Nielsen, S. N., Kuhnt, W., Holbourn, A., Garbe-Schönberg, D., and Andersen, N.: Morphological, geochemical, and ecological differences of the extant menardiform planktonic foraminifera Globorotalia menardii and Globorotalia cultrata, Mar. Micropaleontol., 74, 96–107, https://doi.org/10.1016/j.marmicro.2010.01.002, 2010.

Reuter, M., Piller, W. E., Harzhauser, M., Kroh, A., and Bassi, D.: Termination of the Arabian shelf sea: Stacked cyclic sedimentary patterns and timing (Oligocene/Miocene, Oman), Sediment. Geol., 212, 12–24, https://doi.org/10.1016/j.sedgeo.2008.09.001, 2008.

Reuter, M., Piller, W. E., Harzhauser, M., Mandic, O., Berning, B., Rögl, F., Kroh, A., Aubry, M. P., Wielandt-Schuster, U., and Hamedani, A.: The Oligo-/Miocene Qom Formation (Iran): evidence for an early Burdigalian restriction of the Tethyan Seaway and closure of its Iranian gateways, Int. J. Earth Sci., 98, 627–650, https://doi.org/10.1007/s00531-007-0269-9, 2009.

Reuter, M., Kern, A. K., Harzhauser, M., Kroh, A., and Piller, W. E.: Global warming and South Indian monsoon rainfall–lessons from the Mid-Miocene, Gondwana Res., 23, 1172–1177, https://doi.org/10.1016/j.gr.2012.07.015, 2013.

Reuter, M., Bosellini, F. R., Budd, A. F., Ćorić, S., Piller, W. E., and Harzhauser, M.: High coral reef connectivity across the Indian Ocean is revealed 6–7 Ma ago by a turbid-water scleractinian assemblage from Tanzania (Eastern Africa), Coral Reefs, 38, 1023–1037, https://doi.org/10.1007/s00338-019-01830-8, 2019.

Ridgwell, A. and Zeebe, R. E.: The role of the global carbonate cycle in the regulation and evolution of the Earth system, Earth Planet. Sc. Lett., 234, 299–315, https://doi.org/10.1016/j.epsl.2005.03.006, 2005.

Rixen, T., Goyet, C., and Ittekkot, V.: Diatoms and their influence on the biologically mediated uptake of atmospheric CO_2 in the Arabian Sea upwelling system, Biogeosciences, 3, 1–13, https://doi.org/10.5194/bg-3-1-2006, 2006.

Rixen, T., Gaye, B., Emeis, K.-C., and Ramaswamy, V.: The ballast effect of lithogenic matter and its influences on the carbon fluxes in the Indian Ocean, Biogeosciences, 16, 485–503, https://doi.org/10.5194/bg-16-485-2019, 2019a.

Rixen, T., Gaye, B., and Emeis, K.: The Monsoon, Carbon Fluxes, and the Organic Carbon Pump in the Northern Indian Ocean, Prog. Oceanogr., 175, 24–39, https://doi.org/10.1016/j.pocean.2019.03.001, 2019b.

Rodriguez, M., Chamot-Rooke, N., Huchon, P., Fournier, M., and Delescluse, M.: The Owen Ridge uplift in the Arabian Sea: Implications for the sedimentary record of Indian monsoon in Late Miocene, Earth Planet. Sc. Lett., 394, 1–12, https://doi.org/10.1016/j.epsl.2014.03.011, 2014.

Rodriguez, M., Bourget, J., Chamot-Rooke, N., Huchon, P., Fournier, M., Delescluse, M., and Zaragosi, S.: The Sawqirah contourite drift system in the Arabian Sea (NW Indian Ocean): A case study of interactions between margin reactivation and contouritic processes, Mar. Geol., 381, 1–16, https://doi.org/10.1016/j.margeo.2016.08.004, 2016.

Rögl, F.: Mediterranean and Paratethys. Facts and hypotheses of an Oligocene to Miocene paleogeography (short overview), Geol. Carpath., 50, 339–349, 1999.

Samtleben, C.: Die Evolution der Coccolithophoriden-GattungGephyrocapsa nach Befunden im Atlantik, PalZ, 54, 91–127, https://doi.org/10.1007/bf02985885, 1980.

Sarmiento, J. L.: Ocean Biogeochemical Dynamics, Princeton University Press, Princeton, New Jersey (US), 528 pp., https://doi.org/10.1515/9781400849079, 2006.

Sarmiento, J. L., Gruber, N., Brzezinski, M. A., and Dunne, J. P.: High-latitude controls of thermocline nutrients and low latitude biological productivity, Nature, 427, 56–60, https://doi.org/10.1038/nature02127, 2004.

Sarr, A.-C., Donnadieu, Y., Bolton, C. T., Ladant, J.-B., Licht, A., Fluteau, F., Laugié, M., Tardif, D., and Dupont-Nivet, G.: Neogene South Asian monsoon rainfall and wind histories diverged due to topographic effects, Nat. Geosci., 15, 314–319, https://doi.org/10.1038/s41561-022-00919-0, 2022.

Schiebel, R., Zeltner, A., Treppke, U. F., Waniek, J. J., Bollmann, J., Rixen, T., and Hemleben, C.: Distribution of diatoms, coccolithophores and planktic foraminifers along a trophic gradient during SW monsoon in the Arabian Sea, Mar. Micropaleontol., 51, 345–371, https://doi.org/10.1016/j.marmicro.2004.02.001, 2004.

Schlitzer, R.: Ocean Data View 5.5.1, https://odv.awi.de (last access: 17 October 2023), 2021.

Schott, F. A. and McCreary, J. P.: The monsoon circulation of the Indian Ocean, Prog. Oceanogr., 51, 1–123, 2001.

Schott, F. A., Xie, S.-P., and McCreary Jr., J. P.: Indian Ocean circulation and climate variability, Rev. Geophys., 47, 3295, https://doi.org/10.1029/2007rg000245, 2009.

Schubert, C. J., Villanueva, J., Calvert, S. E., Cowie, G. L., Rad, U. von, Schulz, H., Berner, U., and Erlenkeuser, H.: Stable phytoplankton community structure in the Arabian Sea over the past 200,000 years, Nature, 394, 563–566, https://doi.org/10.1038/29047, 1998.

Schueth, J. D. and Bralower, T. J.: The relationship between environmental change and the extinction of the nannoplankton Discoaster in the early Pleistocene, Paleoceanography, 30, 863–876, https://doi.org/10.1002/2015pa002803, 2015.

Sexton, P. F. and Norris, R. D.: High latitude regulation of low latitude thermocline ventilation and planktic foraminifer populations across glacial–interglacial cycles, Earth Planet. Sc. Lett., 311, 69–81, https://doi.org/10.1016/j.epsl.2011.08.044, 2011.

Shimmield, G. B.: Can sediment geochemistry record changes in coastal upwelling palaeoproductivity? Evidence from northwest Africa and the Arabian Sea, Geological Soc. Lond. Special Publ., 64, 29–46, https://doi.org/10.1144/gsl.sp.1992.064.01.03, 1992.

Shipboard Scientific Party: Site 722, Proceedings of the Ocean Drilling Program, Initial Reports, 117, 255–317, https://doi.org/10.2973/odp.proc.ir.117.107.1989, 1989.

Sigman, D. M. and Fripiat, F.: Nitrogen Isotopes in the Ocean, in: Encyclopedia of Ocean Sciences, Third Edition, edited by: Cochran, J. K., Bokuniewicz, H. J., and Yager, P. L., 263–278, https://doi.org/10.1016/b978-0-12-409548-9.11605-7, 2019.

Smart, C. W., Thomas, E., and Ramsay, A. T. S.: Middle–late Miocene benthic foraminifera in a western equatorial Indian Ocean depth transect: Paleoceanographic implications, Palaeogeogr. Palaeocl., 247, 402–420, https://doi.org/10.1016/j.palaeo.2006.11.003, 2007.

Sokal, R. R. and Rohlf, F. J.: Biometry, 3rd ed., W. H. Freeman and Company, ISBN 9780716724117, 1995.

Sosdian, S. M. and Lear, C. H.: Initiation of the Western Pacific Warm Pool at the Middle Miocene Climate Transition?, Paleoceanogr. Paleocl., 35, e2020PA003920, https://doi.org/10.1029/2020pa003920, 2020.

Spezzaferri, S.: Planktonic foraminiferal paleoclimatic implications across the Oligocene-Miocene transition in the oceanic record (Atlantic, Indian and South Pacific), Palaeogeogr. Palaeocl., 114, 43–74, https://doi.org/10.1016/0031-0182(95)00076-x, 1995.

Stramma, L., Johnson, G. C., Sprintall, J., and Mohrholz, V.: Expanding Oxygen-Minimum Zones in the Tropical Oceans, Science, 320, 655–658, https://doi.org/10.1126/science.1153847, 2008.

Suess, E.: Particulate organic carbon flux in the oceans—surface productivity and oxygen utilization, Nature, 288, 260–263, https://doi.org/10.1038/288260a0, 1980.

Taucher, J., Bach, L. T., Prowe, A. E. F., Boxhammer, T., Kvale, K., and Riebesell, U.: Enhanced silica export in a future ocean triggers global diatom decline, Nature, 605, 696–700, https://doi.org/10.1038/s41586-022-04687-0, 2022.

ThiDieuVu, H. and Sohrin, Y.: Diverse stoichiometry of dissolved trace metals in the Indian Ocean, Sci. Rep., 3, 1745, https://doi.org/10.1038/srep01745, 2013.

Toggweiler, J. R., Druffel, E. R. M., Key, R. M., and Galbraith, E. D.: Upwelling in the Ocean Basins North of the ACC: 1. On the Upwelling Exposed by the Surface Distribution of $\Delta^{14}C$, J. Geophys. Res.-Oceans, 124, 2591–2608, https://doi.org/10.1029/2018jc014794, 2019.

Tomczak, M. and Godfrey, J. S.: Hydrology of the Indian Ocean, edited by: Tomczak, M. and Godfrey, J. S., Daya Publishing House, 199–214, ISBN 8170353068, 2003.

Tripathi, S., Tiwari, M., Lee, J., Khim, B.-K., Pandey, D. K., Clift, P. D., Kulhanek, D. K., Andò, S., Bendle, J. A. P., Aharonovich, S., Griffith, E. M., Gurumurthy, G. P., Hahn, A., Iwai, M., Kumar, A., Kumar, A. G., Liddy, H. M., Lu, H., Lyle, M. W., Mishra, R., Radhakrishna, T., Routledge, C. M., Saraswat, R., Saxena, R., Scardia, G., Sharma, G. K., Singh, A. D., Steinke, S., Suzuki, K., Tauxe, L., Xu, Z., and Yu, Z.: First evidence of denitrification

vis-à-vis monsoon in the Arabian Sea since Late Miocene, Sci. Rep., 7, 43056, https://doi.org/10.1038/srep43056, 2017.

Tudhope, A. W., Lea, D. W., Shimmield, G. B., Chilcott, C. P., and Head, S.: Monsoon Climate and Arabian Sea Coastal Upwelling Recorded in Massive Corals from Southern Oman, Palaios, 11, 347, https://doi.org/10.2307/3515245, 1996.

Ustick, L. J., Larkin, A. A., Garcia, C. A., Garcia, N. S., Brock, M. L., Lee, J. A., Wiseman, N. A., Moore, J. K., and Martiny, A. C.: Metagenomic analysis reveals global-scale patterns of ocean nutrient limitation, Science, 372, 287–291, https://doi.org/10.1126/science.abe6301, 2021.

Villa, G., Fioroni, C., Pea, L., Bohaty, S., and Persico, D.: Middle Eocene–late Oligocene climate variability: Calcareous nannofossil response at Kerguelen Plateau, Site 748, Mar. Micropaleontol., 69, 173–192, https://doi.org/10.1016/j.marmicro.2008.07.006, 2008.

Volk, T. and Hoffert, M. I.: Ocean Carbon Pumps: Analysis of Relative Strengths and Efficiencies in Ocean-Driven Atmospheric CO_2 Changes, in: The Carbon Cycle and Atmospheric CO_2: Natural Variations Archean to Present, vol. 32, edited by: Sundquist, E. T. and Broecker, W. S., 99–110, https://doi.org/10.1029/gm032p0099, 1985.

Wade, B. S. and Bown, P. R.: Calcareous nannofossils in extreme environments: The Messinian Salinity Crisis, Polemi Basin, Cyprus, Palaeogeogr. Palaeocl., 233, 271–286, https://doi.org/10.1016/j.palaeo.2005.10.007, 2006.

Wang, D., Gouhier, T. C., Menge, B. A., and Ganguly, A. R.: Intensification and spatial homogenization of coastal upwelling under climate change, Nature, 518, 390–394, https://doi.org/10.1038/nature14235, 2015.

Wei, W. and Wise, S. W.: Biogeographic gradients of middle Eocene-Oligocene calcareous nannoplankton in the South Atlantic Ocean, Palaeogeogr. Palaeocl., 79, 29–61, 1990.

Westerhold, T., Marwan, N., Drury, A. J., Liebrand, D., Agnini, C., Anagnostou, E., Barnet, J. S. K., Bohaty, S. M., Vleeschouwer, D. D., Florindo, F., Frederichs, T., Hodell, D. A., Holbourn, A. E., Kroon, D., Lauretano, V., Littler, K., Lourens, L. J., Lyle, M., Pälike, H., Röhl, U., Tian, J., Wilkens, R. H., Wilson, P. A., and Zachos, J. C.: An astronomically dated record of Earth's climate and its predictability over the last 66 million years, Science, 369, 1383–1387, https://doi.org/10.1126/science.aba6853, 2020.

Woodruff, F. and Savin, S. M.: Miocene deepwater oceanography, Paleoceanography, 4, 87–140, https://doi.org/10.1029/pa004i001p00087, 1989.

Woodward, E. M. S., Rees, A. P., and Stephens, J. A.: The influence of the south-west monsoon upon the nutrient biogeochemistry of the Arabian Sea, Deep-Sea Res. Pt. II, 46, 571–591, https://doi.org/10.1016/s0967-0645(98)00118-0, 1999.

Yang, X., Groeneveld, J., Jian, Z., Steinke, S., and Giosan, L.: Middle Miocene Intensification of South Asian Monsoonal Rainfall, Paleoceanogr. Paleocl., 35, e2020PA00385, https://doi.org/10.1029/2020pa003853, 2020.

Yao, Z., Shi, X., Guo, Z., Li, X., Nath, B. N., Betzler, C., Zhang, H., Lindhorst, S., and Miriyala, P.: Weakening of the South Asian summer monsoon linked to interhemispheric ice-sheet growth since 12 Ma, Nat. Commun., 14, 829, https://doi.org/10.1038/s41467-023-36537-6, 2023.

You, Y.: Seasonal variations of thermocline circulation and ventilation in the Indian Ocean, J. Geophys. Res.-Oceans, 102, 10391–10422, https://doi.org/10.1029/96jc03600, 1997.

You, Y.: Intermediate water circulation and ventilation of the Indian Ocean derived from water-mass contributions, Journal of Marine Research 56, 5, https://elischolar.library.yale.edu/journal_of_marine_research/2299 (last access: 2 November 2023), 1998.

You, Y. and Tomczak, M.: Thermocline circulation and ventilation in the Indian Ocean derived from water mass analysis, Deep-Sea Res. Pt. Oceanogr. Res. Pt. I, 40, 13–56, https://doi.org/10.1016/0967-0637(93)90052-5, 1993.

Young, J.: Size variation of Neogene Reticulofenestra coccoliths from Indian Ocean DSDP Cores, J. Micropalaeontol., 9, 71–85, https://doi.org/10.1144/jm.9.1.71, 1990.

Young, J. R.: Neogene, in: Calcareous Nannofossil Biostratigraphy, edited by: Bown, P. R., 225–265, ISBN 9780412789700, 1998.

Zhang, Z., Ramstein, G., Schuster, M., Li, C., Contoux, C., and Yan, Q.: Aridification of the Sahara desert caused by Tethys Sea shrinkage during the Late Miocene, Nature, 513, 401–404, https://doi.org/10.1038/nature13705, 2014.

Zhuang, G., Pagani, M., and Zhang, Y. G.: Monsoonal upwelling in the western Arabian Sea since the middle Miocene, Geology, 45, 655–658, https://doi.org/10.1130/g39013.1, 2017.

Zweng, M. M., Reagan, J. R., Seidov, D., Boyer, T. P., Locarnini, M. M., Garcia, H. E., Mishonov, A. V., Baranova, O. K., Weathers, K. W., Paver, C. R., and Smolyar, I.: World ocean atlas 2018, Volume 2: Salinity, edited by: Mishonov, A., 50 pp., https://www.ncei.noaa.gov/access/world-ocean-atlas-2018/ (last access: 12 October 2023), 2019.